Bottom Stress Estimates and their Prediction on the Northern California Continental Shelf during CODE-1: The Importance of Wave–Current Interaction[1]

WILLIAM D. GRANT AND ALBERT J. WILLIAMS, III

Ocean Engineering Department, Woods Hole Oceanographic Institution, Woods Hole, MA 02543

SCOTT M. GLENN[2]

Shell Development Company, Houston, Texas

(Manuscript received 7 July 1983, in final form 21 November 1983)

ABSTRACT

High quality near-bottom boundary layer measurements obtained at a midshelf location (90 m water depth) in the CODE region off Northern California are described. Bottom tripod velocity measurements and supporting data obtained during typical spring and early summer conditions (June 1981 during CODE-1) are analyzed to obtain both velocity profiles and mean bottom stress and bottom roughness estimates. During the time period described, the mean near-bottom (<2 m) velocity profiles are highly logarithmic ($R > 0.997$) approximately 30 percent of the time. Effects induced by unsteadiness from internal waves result in some degradation of the profiles ($0.96 \leq R \leq 0.997$) the rest of the time. Mean stress profiles indicate the logarithmic layer is approximately a constant-stress layer. The near-bottom flow field is composed of mean currents and oscillatory currents due to swell. Typical mean u_* values estimated from measurements greater than 30 cm above the bottom have magnitudes of 0.5–1.0 cm s^{-1}. Mean stress values are three to seven times larger than expected from predictions using a typical smooth-bottom drag coefficient and one-and-one-half to three-and-one-half times larger than expected for predictions using a drag coefficient based on the observed rough bottom. Corresponding z_0 values have magnitudes of approximately 1 cm, an order of magnitude larger than the observed physical bottom roughness. These values are demonstrated to be consistent with those expected from theoretical models for combined wave and current flows. The u_* values estimated from the CODE-1 data and predicted by the Grant and Madsen model typically agree within 10–15 percent.

The waves influencing the midshelf bottom-stress estimates are 12–20 second swell associated with distant Pacific storms. These waves are present over most of the year. The results demonstrate that waves must be taken into account in predicting bottom stress over the Northern California Shelf and that these predictions can be made using existing theory.

1. Introduction

The importance of bottom shear stress to the dynamics controlling the vertical velocity structure in the bottom boundary layer and the wind driven circulation on the continental shelf is generally recognized (e.g., Csanady, 1978; Smith and Long, 1976; Allen, 1980; Brink and Allen, 1978). There is, however, considerable uncertainty as to the importance of bottom stress relative to other terms in the governing equations for wind-driven shelf flows over different regions of the continental shelf. This uncertainty stems from the lack of direct estimates of bottom stress over various regions of continental shelves as well as a lack of understanding of the key processes contributing to the spatial and temporal variability of the bottom stress. This latter problem is particularly crucial since the determination of the bottom stress associated with the synoptic-band, wind driven circulation (typically 2–10 day time scales and kilometer length scales) for example, or for the vertical velocity structure, (typically time scales of minutes to hours and length scales of centimeters to meters) require very different types of temporal and spatial averaging. This averaging can be carried out properly only if the length and time scales of the key processes contributing to the stress are known.

During the recent Coastal Ocean Dynamics Experiment, CODE (Allen *et al.*, 1982) an opportunity was presented to investigate the structure of the bottom stress field on a geomorphologically simple continental shelf in the context of a large comprehensive continental shelf experiment. The overall objective of CODE is to identify and study the important dynamical processes that govern the wind driven motion of coastal waters over the continental shelf. The initial effort of the four-year research program is to obtain high quality datasets of all the relevant physical variables needed to construct accurate kinematic and dynamic descrip-

[1] Woods Hole Oceanographic Institution Contribution No. 5432.
[2] Former affiliation: Woods Hole Oceanographic Institution.

tions of the response of shelf water to strong wind forcing in the 2–10 day synoptic scale. Two small-scale densely instrumented field experiments of four-months duration each, in the spring of 1981 and 1982 (CODE-1 and CODE-2), were designed to accomplish this task. The major observational elements of CODE were: 1) moored arrays instrumented to measure wind, solar radiation, currents, temperature, conductivity, bottom pressure and near-bottom currents; 2) shipboard observations of temperature, conductivity, currents, wind and surface fluxes; and 3) aircraft observations of wind, wind stress, sea surface temperature, surface drifter motion and atmospheric parameters. In addition, satellite-derived sea surface temperature data were collected and measurements made of wind, atmospheric pressure and sea level at appropriate coastal stations and environmental buoys.

This paper discusses results of the near-bottom current measurements made as part of the Bottom Boundary Layer and Bottom Stress Component of CODE-1. The motivation behind what is reported here is to establish the ability to predict accurately the local mean stress as a function of the typical processes occurring on the continental shelf at the CODE location. This ability allows one to look at differences in these processes over the shelf and to predict the associated variability in bottom stress, rather than having to make detailed measurements at many locations on the shelf from which stress can be directly estimated.

a. Bottom Boundary Layer–Bottom Stress Component of CODE

The Bottom Boundary Layer and Bottom Stress Component of CODE has as two of its primary objectives in CODE-1: 1) the resolution of the bottom stress on the shelf to determine the physical processes having a major influence on its magnitude and spatial and temporal variability; and 2) the development and testing of an appropriate model for prediction of stress and the associated near-bottom velocity profile as a function of easily measured quantities characterizing the flow and bottom conditions. The experimental program enacted to carry out these objectives was composed of two current measurement programs, a long-term, sparsely sampled component and a short-term, densely sampled component, along with a detailed survey effort to characterize the micro- and macro-physiography of the continental shelf in the CODE area.

The long-term component consisted of the deployment of a single USGS GEOPROBE tripod (Cacchione and Drake, 1979) at a midshelf location in the CODE-1 array for time periods of up to two months. This tripod measured velocity profiles every two hours along with a suite of supporting variables. These measurements are being analyzed to yield a long-time series of stress and also of the near bottom flow. The long-term component was maintained for the better part of one year during CODE and approximately 15 months prior to CODE.

A short-term (approximately two weeks in CODE-1) experiment was nested within this long-term monitoring program. This short-term experiment provides detailed measurements of the relevant quantities required to resolve the role of key processes contributing to the bottom stress and to make accurate estimates of vertical profiles of stress and near-bottom horizontal velocity. These measurements provide a high-quality dataset from which to test models for prediction of the bottom velocity profile and stress from knowledge of several easily measured flow and bottom variables [i.e., objective 2) above]. The short-term experiments also were used 1) to examine the spatial variability of the bottom stress field on a local scale of hundreds of meters and on a larger scale in the cross-shelf direction and 2) to determine the applicability of the profile technique used to make stress estimates from the long-term GEOPROBE measurements. The short-term component consisted of an array of WHOI BASS W bottom tripods deployed for periods of 3–5 days. These tripods sampled a suite of variables and three components of velocity at four levels above the seabed using a repeating sequence of continuous measurements for up to several hours and a shut-off period of approximately an hour.

b. Boundary-layer processes on the continental shelf

Numerous observations of bottom flows on continental shelves, including the CODE site, demonstrate that typically the near-bottom flow field is composed of velocity components due to both surface waves and low-frequency currents (tidally, wind, or density driven). Other phenomena occurring on the shelf that have the potential to influence the near-bottom flow structure include: 1) stratification due to temperature and salinity, 2) stratification due to suspended sediment, 3) moveable bed effects (i.e., ripples and near-bed sediment transport, bioturbation), 4) internal waves and 5) topographically complex bottoms.

Several of the above phenomena have similar effects on the mean velocity profile. For example, both surface waves and moveable-bed phenomena affect the roughness felt by the flow measured tens of centimeters above the bottom. In both cases, the roughness length is increased by an order of magnitude, or more, over the roughness attributed to the sediment grain size. Failure to correct measured near-bottom velocity profiles for stratification effects leads to an erroneous increase in the boundary roughness and in the value of von Karman's constant (Grant and Glenn, 1983). The presence of high-frequency internal waves superimposed on a mean flow results in an apparent "kink" or change in slope in the velocity profile, both of which can look similar to the effects of upstream topography. More-

over, at any time several of the above phenomena may be present and affect the flow simultaneously, causing significant changes to the slope of the measured mean velocity profile near the bed.

Thus, for the results of a bottom boundary-layer experiment to be useful it is of utmost importance to make measurements that allow unambiguous and quantitative assessment of the phenomena causing the observed velocity structure and affecting the associated estimated quantities such as velocity profile distributions and bottom stress. Models are helpful to distinguish between the effects of various phenomena present and to determine the important quantities that characterize a particular process and how precisely they must be measured. Extensive use of recently developed models was made to design the CODE experiments. Theoretical models for the near-bottom flow field and bottom shear stress under combined wave and current flows have been developed by Grant and Madsen (1979) and Smith (1977). Both of these models include nonlinear interaction between the wave and current flows and give solutions for the wave and current kinematics and associated boundary shear stress. Each model partitions the bottom boundary layer into two distinct boundary layer regions. A wave boundary layer region, limited in vertical extent by its short diffusion time scale, is nested within a larger mean-flow boundary layer. These models predict, for the combined flow over rough bottoms, that the mean shear stress above the wave boundary layer is enhanced by the presence of the waves: The Grant and Madsen (1979) model also predicts that the flow above the wave boundary layer "feels" an increased roughness, termed an apparent roughness. This apparent roughness depends on the characteristics of the turbulent wave boundary layer as well as the physical bottom roughness associated with moveable-bed effects (e.g., bedforms or sediment transport, or animal mounds).

The Grant and Madsen (1979) model has recently been extended to include the phenomena (1)–(3) above (Grant and Madsen, 1982; Glenn, 1983; Grant and Glenn, 1983). The results of the extensions indicate that the inclusion of flow–sediment interaction through moveable-bed effects and self-stratification of the near-bottom flow by suspended sediment has pronounced and important influences on the near-bottom velocity profile; these influences are likely to be most important during storm flows. Thus, it is highly desirable to have separate datasets for conditions 1) where wave–current interaction is the only major process, and 2) where the wave–current interaction is occurring with sediment transport.

Results from the short-term CODE-1 experiment for the mean and surface wave components of the flow field and associated stress estimates are presented in this paper. Here, mean refers to time averages of velocity over 10 to 20 minutes for reasons discussed in the paper. The paper provides a quantitative and unambiguous comparison of the model for near-bottom flow and stress of Grant and Madsen (1979) with data where wave–current interaction is the only major dynamical contribution to the bottom stress. Qualitative agreement with the predictions of the Grant and Madsen (1979) and Smith (1977) models of mean shear stress, roughness and mean velocity profiles (above the wave boundary layer) are available from field measurements by Cacchione and Drake (1982) and from laboratory measurements by Bakker and van Doorn (1978) and Kemp and Simons (1982). Although these measurements provide encouraging agreement with aspects of the models, none of these datasets contain the required control for an unambiguous test of the models.[3] This paper addresses in detail only the prediction of the velocity profile and *mean* stress at a point on the shelf as a function of the processes occurring there. The description of the overall bottom boundary-layer structure, the large-scale spatial and long-term temporal variability in the bottom stress, turbulent structure, and the general description of the stress field on the shelf will be addressed in future papers and reports.

2. Experimental details

a. Site and flow description

The CODE site is located along the northern California shelf between Point Arena and Point Reyes. The measurements described here were made during CODE-1 in early June 1981 in 90 m of water at the vicinity of station C3 (38°37.2'N, 123°28.4'W) along the central line of the small-scale CODE-1 array (see Figs. 1 and 2). The prevailing winds along the northern California coast during late spring and summer are from the northwest and are favorable for upwelling. The wind speed is highly variable and over the middle and inner shelf there is pronounced diurnal variability in the longshore wind caused by the local sea breeze. The wind during the CODE-1 Bottom Boundary Layer/Bottom Stress cruise was consistent with this prevailing wind pattern with speeds of 25–40 kt out of the northnorthwest. During the experiments, the mean near-bottom flow varied in both magnitude and direction. In contrast, the long waves driving the oscillatory component of the bottom flow are southern or western ocean swell and are relatively constant. Thus, from the dataset it is possible to examine, at the same site, a range of wave and wind-driven flows with differing relative strengths and directions.

[3] A reanalysis of the GEOPROBE storm data taken in the Norton Sound (Cacchione and Drake, 1982) by Wiberg and Smith (1983) show that by making zero shifts of the velocity profiles, better agreement than Cacchione and Drake (1982) found is achieved with roughness-length estimates from theories of Grant and Madsen (1979) and Smith (1977). The data quality is still limited by the one-minute record lengths, however.

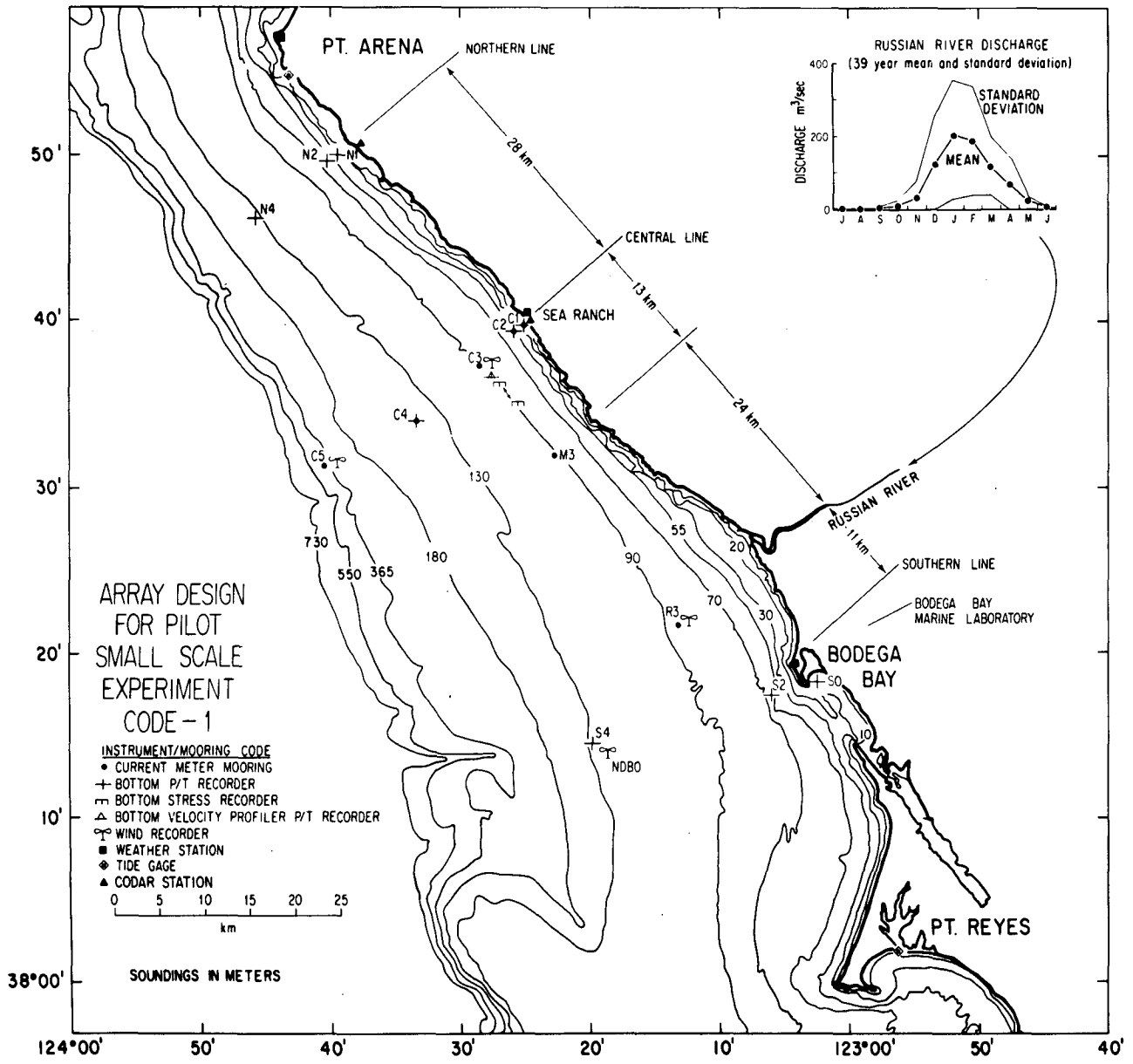

FIG. 1. Locations of the principal CODE-1 mooring sites along north (N), central (C) and south (S) cross-shelf transects.

b. Instrumentation and measurements

1) NEAR-BOTTOM VELOCITY MEASUREMENTS

Near-bottom velocity profiles were measured using sets of four vertically stacked, acoustic-travel-time current meters mounted on tripods. The current meter electronics were designed and built by A. Williams and R. Koehler at Woods Hole Oceanographic Institution and are described by Williams and Koehler (in preparation). The current sensors measure velocity averaged over a 15-cm path length along four separate intersecting axes inclined at 45° to the vertical. For initial processing, three axes are picked from the four depending on the flow direction. These three axes are rotated, using a computer algorithm, into u, v and w components in a rectangular coordinate system where w is the vertical component, and u and v are the two horizontal components. The current meter has been calibrated in both steady and oscillatory flow (Grant, *et al.*, in preparation); it has a 0.3 cm s^{-1} precision in the field (with a sensitivity of 0.06 cm s^{-1}), and excellent vertical and horizontal cosine response. The current sensor geometry has been designed to minimize flow disturbance from the sensor frame from any direction, since the instantaneous flow vector associated with

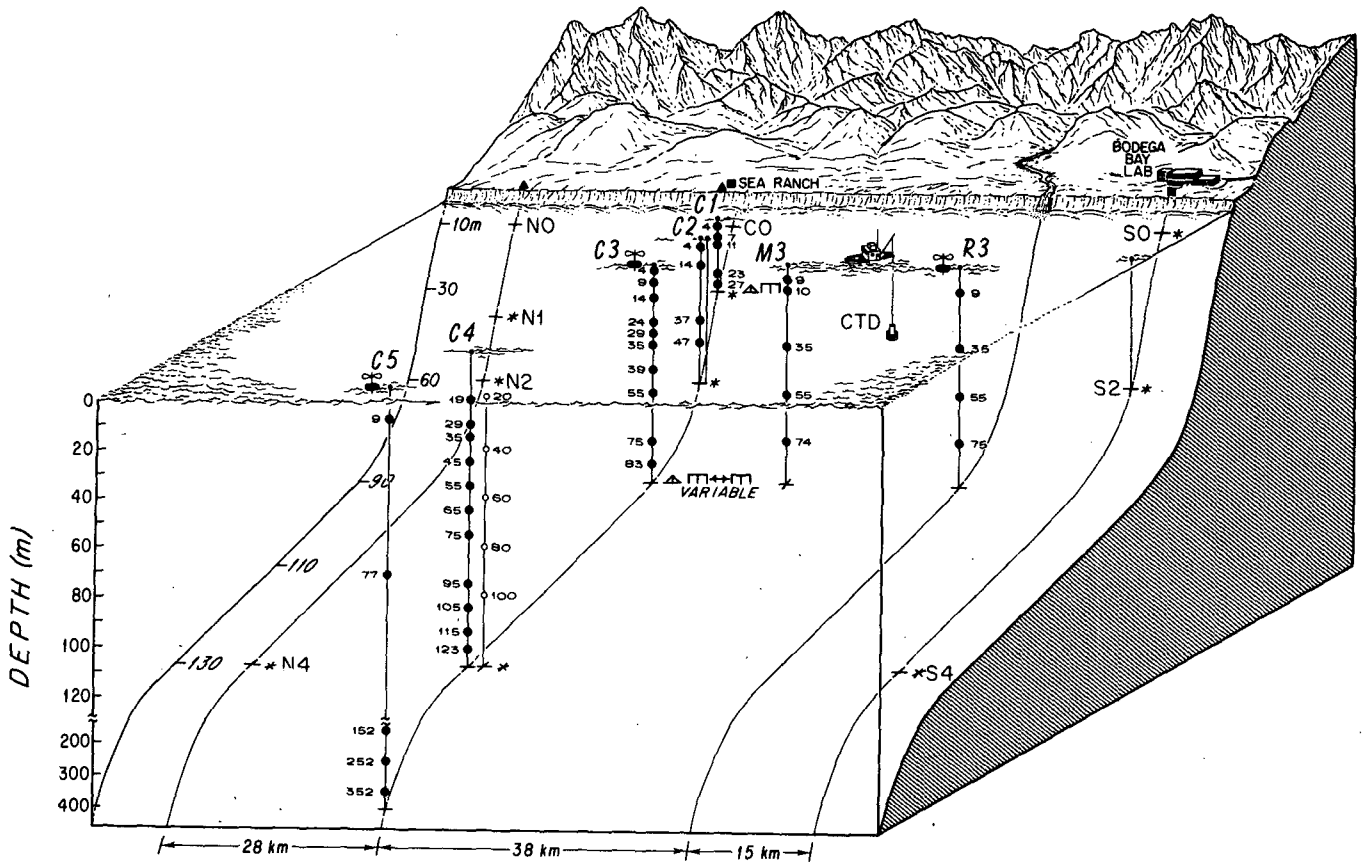

FIG. 2. Schematic of CODE-1 small-scale array. Current meter locations are identified by (dots); wind buoys (); temperature/conductivity (open circles); bottom stress (⋀, ⊓); pressure (asterisks); CODAR (solid triangles); and meteorological stations (solid squares). Mooring designations are also indicated.

combined wave and current flows continually changes direction.

The velocity sensors were mounted on bottom tripods at approximately 30, 55, 105 and 205 cm above the bottom. These actual heights were later corrected for initial tripod settlement into the bottom as monitored by a mechanical gauge or 1 MHz echo sounder. In addition to the velocity sensors, the tripods contained instruments to monitor variables required in the analysis and interpretation of the velocity data. These instruments and their locations relative to the bottom are described below and listed in Table 1 along with a summary of the velocity sensors. The tripods have structural members ~ 2.5 cm in diameter which are spread far from the sensors to minimize possible flow disturbance. Velocity spectra are routinely checked for evidence of flow disturbance.

Two different sampling schemes on two different tripods were employed during the experiment because of the interest in making both a large number of measurements at fast sampling rates and obtaining a long time series. One tripod sampled at 5 Hz, telemetered its data back to the ship and was left at one point for approximately 4 days. This fast-sampling tripod employed a variable-length sampling duration controlled from the ship; typically, the repeating sequence used was 120 minutes on, 60 minutes off and then a sequence of 40 minutes on–40 minutes off, repeated twice. A second tripod contained fewer support instruments and sampled at 2 Hz; this tripod recorded *in situ* for up to six hours. It was deployed at different locations within one-half to one kilometer of the stationary telemetering tripod.

2) SUPPORT MEASUREMENTS

A pressure sensor (Paroscientific digiquartz), compass, pitch and roll sensors, and three thermistors were mounted on all tripods (Table 1). The pressure sensors were used to determine both water depth and as an independent measure of the surface waves. The thermistors were used in conjunction with CTD profiles to monitor possible near-bottom stratification and changes in temperature associated with advection of bottom water. Pitch and roll sensors were used to monitor tripod orientation relative to the bottom and to monitor any settlement. The telemetering tripod also contained two transmissometers (Sea Tech; ¼-m

TABLE 1. Tripod measurements and boundary layer support measurements.

Sensor	Measurement/parameters	Location	Sampling rate
Acoustic travel time current meter (15 cm averaging volume)	u, v, w	30, 55, 105, 205 cm tripod	5 Hz
Pressure	Pressure/H, T, h, u_w, v_w	105 cm; tripod	5 Hz
Transmissometer (¼ meter)	Light attenuation/total suspended concentration	75 cm, 175 cm; tripod	5 Hz
Thermistors	Temperature (T°C)	50, 100, 200 cm; tripod	5 Hz
Compass	Direction	2½ m; tripod	5 Hz
Pitch/roll	Tripod tilt	2½ m; tripod	5 Hz
Bottom locator (mechanical or acoustic 1 MHz)	Bottom location	Bottom; tripod	N/A 1 s^{-1}
Camera	Bottom photograph	Tripod	1 per half hour
Vector measuring current meter	u, v, T	2½, 5½, 7½ m C3 mooring	Vector averaged every 4 min
CTD (NBIS) (SCIMP)	Conductivity, temperature, pressure	Surface to within ½ meter off bottom; CODE site	Selected intervals
Side scan	Bottom topography	CODE site	Selected intervals
Box cores	Bottom topography, benthic biota, sediment	CODE site	Selected intervals
Suspended sediment	Water samples, sediment concentration	CODE site	Selected intervals

path length) to monitor suspended sediment concentration. All instruments on the tripods were sampled simultaneously with the velocity sensors. Over the course of the experiments CTD profiles to within 0.5 m of the bottom were systematically taken at tripod locations to determine the location of the bottom mixed layer and possible stratification of the bottom boundary layer.

Geological and biological data were collected during CODE-1 and other cruises in the region. Bottom topography was measured so that macro- and microtopography could be determined in the vicinity of the tripod locations. Side-scan sonar tracks were run to resolve large-scale features relative to the tripod location. Bottom cameras and box cores at the tripod sites were used to resolve the microtopography and to sample the benthic biota responsible for generating the microtopography. The results of these latter measurements are reported by Cacchione *et al.* (1983). The bottom-sediment distribution at the site was mapped using tripod samples, grab samples, and box cores. The distribution also is summarized by Cacchione *et al.* Water samples taken during hydrographic transects allowed the suspended sediment to be related to the bottom sediments and the transmissometer measurements.

Low-frequency characteristics of the flow, internal waves and vertical profiles of velocity through the bottom boundary layer were determined from measurements made, using arrays of vector-measuring current meters (VMCMs) deployed at the CODE site. In CODE-1, during the boundary layer experiments a densely spaced (in the vertical), current meter mooring was deployed by C. Winant and R. Davis in 90 m of water at C3, with VMCMs at 4, 9, 14, 24, 29, 35, 39, 55, 75 and 83 m below the surface (Allen *et al.*, 1982). During the short-term bottom stress experiments a near-bottom mooring was deployed with VMCMs at 2.5, 5.5, and 7.5 m above the bottom. This mooring was designed to provide continuity between the tripod measurements and the large VMCM array. Temperature was also measured in the large VMCM array.

c. *Data analysis*

1) SELECTION

Approximately 4 days of high-frequency boundary layer data was taken at C3 during the CODE-1 experiment. In addition, three simultaneous deployments of two tripods at C3 within a kilometer of each other provide replicate data on the near-bottom flow. *Representative* measurements over a 15-h time period from this four day period taken with the telemetering (5 Hz sampling rate) tripod are discussed here. An analysis and comparison with model predictions is presented.

During this time period data quality is high and good support measurements are available.

2) PROCESSING OF VELOCITY DATA

The velocity data from each travel-time axis on the acoustic current meters are recorded on cassette tape. These data are unpacked onto 9-track tape, each axis is edited to remove any spurious electronic "glitches" in the data and the calibrated offset for each axis is subtracted. The data from each axis are rotated into a streamline turbulent velocity system such that

$$\mathbf{u} = (u + u'; v'; w'), \tag{1}$$

where u is the mean downstream velocity, u', v' are the fluctuating components of velocity in the streamwise and cross-stream directions respectively and w' is the fluctuating component of velocity normal to the streamline.

The magnitude of the mean velocity is defined as

$$u = \frac{1}{T}\left| \int_t^{t+T} \mathbf{u}(t)dt \right|, \tag{2}$$

where T is the averaging time. Spectral analysis of the resulting velocity signal demonstrates that it is composed of fluctuations associated with high-frequency turbulence, surface waves, internal waves, and low-frequency shelf currents. Thus, in (2) T is chosen to be longer than the surface wave period but significantly less than the internal wave period. The characteristics of the internal waves and surface waves are best determined from measurements independent of the tripod velocity records since the latter measurements contain contributions from the full range of frequencies present.

The surface wave period and velocity were calculated independently from the velocity measurements by using the pressure signal. Linear wave theory was used to convert the pressure records to the equivalent bottom velocity. Extensive comparisons made between one-dimensional wave spectra based on the measured velocity from the current meters and the velocity calculated from the pressure records using linear theory demonstrate that the two techniques yield nearly identical results. Wave period was determined by keeping account of zero crossings in the pressure record. Wave direction was determined using the pressure sensor and the two horizontal velocity components at the same height (e.g., Nagata, 1964). Although the vertical velocity could be substituted for pressure in these directional wave calculations, the pressure is preferred because of its superior signal-to-noise ratio relative to the vertical velocity records.

The internal waves are more difficult to quantify on a wave-by-wave basis. Analysis of velocity and temperature records from the VMCM mooring at the site (see Fig. 2) shows the existence of individual wave packets propagating onto the shelf. These packets are intermittent; their presence is readily determined from the temperature records and the period of individual waves can be determined approximately from the temperature fluctuations.

The turbulent contribution to the velocity signal at high frequencies can be resolved from measurements with the three axis acoustic current meters. The current meters are capable of measuring well into the inertial subrange for the flow speeds observed and the sampling rate used; the high-wavenumber cutoff in resolution is set by the averaging volume of the sensors. The characteristics of the most energetic turbulent structure of the near-bottom flow are difficult to pick out because of the close proximity of the peak in the swell kinetic energy and the turbulent kinetic energy. Separation of the two signals requires careful assumptions concerning linear wave theory and is not discussed here.

To investigate whether an inertial subrange exists, the spectral density for the velocity components in the turbulent coordinate system corresponding to (1) is explored. Frequency can be converted to wavenumber by applying a frozen-turbulence assumption. Application of the frozen-turbulence assumption requires that the turbulent time scale of an eddy with a particular wavenumber be much greater than the time to advect the eddy by the measurement probe (Lumley, 1965). For a given wavenumber k this requirement can be expressed as $(kl)^{1/3} \gg u'/u_D$, where l is the scale of the energy-containing eddies and u_D is the advection velocity. In the inertial subrange $kl > 1$ and therefore u'/u_D must be $\ll 1$. The frozen-turbulence assumption must be applied carefully in high-frequency bands when large velocity fluctuations associated with surface waves are present. Lumley and Terray (1983) and Donelan *et al.* (1983), in studies of the marine surface layer, have found that the entire subrange spectral characteristics may be affected when large orbital wave velocities relative to the mean flow are present.

For typical spring conditions at the midshelf CODE site the ratio of rms orbital wave velocity to mean flow velocity at the bottom is small and at the lower-frequency end of the inertial subrange the mean velocity adequately approximates the advection velocity and the effect of waves on the inertial subrange is negligible. (This point will be discussed further.) For horizontal kinetic-energy spectra any possible distortion of the inertial subrange of the spectrum (caused by the presence of surface waves) is difficult to pick out because of the dominance of the wave peak over the turbulent kinetic energy. The wave peak is not a problem for the vertical kinetic energy since the near-bottom vertical orbital wave velocity in the lower two meters is small. Thus, only w' spectral density estimates are used to examine the high-frequency end of the velocity spectrum in the bottom two meters.

3) PROFILE ANALYSIS

The time-averaged near-bottom velocity profile in a neutral, turbulent boundary layer over a topograph-

ically simple bottom, characteristic of the CODE site, is predicted to follow a logarithmic velocity profile given by

$$u = \frac{u_*}{\kappa} \ln \frac{z - \delta_D}{z_0}, \tag{3}$$

where u is the mean horizontal velocity, κ is von Karman's constant, z the height above the bottom, z_0 the bottom roughness, δ_D is the displacement height and u_* is the shear velocity associated with the mean flow; $u_* = (|\tau_c|\rho^{-1})^{1/2}$ where $|\tau_c|$ is the magnitude of the time-averaged bottom stress and ρ is the fluid density.

The processed velocity time series at each level were first time averaged over intervals of approximately 5, 10, 15 and 20 min using a running average. The flow must be referenced to the average bottom location around the tripod, not simply the bottom at the point below the velocity sensor. A rough estimate of the maximum uncertainty in the relative vertical position of the bottom location for these experiments is about 5 cm. This estimate is arrived at by considering the standard deviation of all bottom location measurements (mechanical gauge and 1 MHz echo sounder), taking into account the resolution of the side scan and the heights of the microtopographic features estimated from bottom photos and box cores. The velocity averages were plotted on a linear scale, and their vertical location above the bottom was shifted upward and downward (referred to as zero shifts) within the range of the 5 cm uncertainty. The best-fit straight line using a least-squares linear regression was fitted to the plotted points for each zero shift for comparison with (3). The profiles were then investigated to determine their sensitivity to zero shifts and for the presence of any curvature. The displacement height estimated from the roughness-element heights (Jackson, 1981) is the same order of magnitude as the zero shifts and was subsequently ignored in further analysis. Profiles passing a set criteria were picked for more detailed analysis to determine bottom stress and roughness using the profile technique as described below.

4) Stress and roughness estimates

The primary goals of the results presented in this paper are to estimate the mean bottom stress for typical CODE-1 conditions needed for making dynamical balances, as described in the Introduction, and to develop and test a predictive model for the bottom stress. The model assumes the near-bottom velocity profile is logarithmic and that the vertical stress distribution in the log layer is approximately constant. Part of testing the model for bottom stress was to evaluate the validity of these assumptions. In addition, the velocity profile given by (3) is specified by the roughness length and shear velocity. Thus, estimates of shear velocity, bottom roughness and vertical profiles of stress were estimated from the measurements. Two indirect techniques can be used to estimate bottom stress. These are the inertial dissipation technique (e.g., Deacon, 1959) and the log-profile technique. Direct estimates of stress can be made using Reynolds stresses. In natural flows when surface waves are present, the results of this technique must be used with caution since error bars on the stress calculations are difficult to estimate. Future analyses will resolve the error-estimation problem and no further discussion of the Reynolds-stress technique will be given here. The stress estimates from the indirect techniques are adequate for the present purposes.

Each of the indirect stress estimates has its advantages and disadvantages. Use of both techniques allows a check on the other since they make use of different characteristics of the velocity signal. The inertial dissipation technique is relatively insensitive to zero shifts, it depends only on a small range of wavenumbers and is insensitive to noise or any signal outside the range of wavenumbers in the portion of the inertial subrange where estimates are made. Stress at each velocity measurement level can be estimated with only minimum assumptions concerning the local mean flow profile. Its major disadvantages are that it requires that potential effects of waves must be taken into account in making error determinations. Also, to estimate roughness lengths some assumption must be made about the relationship between stress and roughness.

The inertial dissipation technique utilizes the relationship between kinetic energy density and wavenumber in the inertial subrange to calculate the stress. In a neutral, locally isotropic, horizontally homogeneous and stationary boundary layer, the one-dimensional vertical kinetic-energy density $\phi_w(k)$ can be expressed in the inertial subrange in terms of the dissipation ϵ as

$$\phi_w(k) = \alpha_3 \epsilon^{2/3} k^{-5/3}, \tag{4}$$

where k is the vertical wavenumber of a turbulent eddy and α_3 is the one-dimensional vertical Kolmogorov constant. In (4) $\phi_w(k)$ is defined in terms of the spectral density in frequency as

$$\phi_w(k) = \frac{1}{2} \frac{\phi'(f)}{2\pi/u}, \tag{5}$$

where $\phi'(f) = S(f)/\Delta f$ in which $S(f)$ is the power spectrum and Δf the band width. The factor of one-half is included in (5) to make $\phi_w(k)$ equivalent to kinetic energy. The Taylor hypothesis has been used to convert frequency to wavenumber. In the near-bottom region the turbulent kinetic-energy balance assumes that dissipation equals production of energy under the assumptions above. Thus, $\epsilon = (-\overline{u'w'})\partial u/\partial z$. If the region is a constant-stress layer, $-\overline{u'w'} = u_*^2$ and u_*^2 can be expressed in terms of the dissipation ϵ as

$$u_*^2 = (\kappa \epsilon z)^{2/3}. \tag{6}$$

Rearranging (4) allows ϵ to be expressed in terms of the spectral density function $\phi_w(k)$ and substituting the result in (6) gives an expression for u_*

$$u_* = \left\{\left[\frac{\phi_w(k)k^{5/3}}{\alpha_3}\right]^{3/2}\kappa z\right\}^{1/3}. \quad (7)$$

Bottom stress and bottom roughness were estimated also from the measured velocity profiles. The velocity profile given by (3) can be rewritten in the form

$$\log z = \frac{\kappa}{2.3u_*}u + \log z_0, \quad (8)$$

which is the equation for a straight line on a plot of $\log z$ versus u. The shear velocity is determined from the slope of the line and the roughness length from the z intercept. It is clear from (8) that the velocity profiles must be considered logarithmic to use the profile technique for estimates of shear velocity and roughness length. Measures of the goodness of fit of a log law to the observed velocity profile are the regression coefficient and standard error. The question of how good the fit must be to accept the profile as logarithmic is still subjective, however. In contrast, evaluation of the confidence bands on the estimates of shear velocity and roughness are more readily quantified. An acceptable confidence band on u_* can be specified and profiles with estimates outside the band are rejected as having too large an uncertainty, and the estimates must be made using another technique.

The confidence bands on the shear-velocity estimates depend on the value of the regression coefficient, the number of current meters and their location in the vertical. A simplified expression for the confidence bands on the shear velocity (e.g., Gross and Nowell, 1983) is

$$\hat{u}_*(1 - e) \leq \hat{u}_* \leq \hat{u}_*(1 + e), \quad (9)$$

where u_* is the estimate of u_* and e is given by

$$e = (t_{\alpha/2,n-2})\left[\frac{1}{n-2}\left(\frac{1-R^2}{R^2}\right)\right]^{1/2}, \quad (10)$$

where t is the Student's t distribution for the $(1 - \alpha)$ confidence interval with $n - 2$ degrees of freedom, n the number of current meters and R the regression coefficient. For a given current meter configuration the acceptable confidence interval depends only on the regression coefficient.

To ensure accurate stress estimates and to keep comparisons between data estimates and model results rigorous we desired to keep the error bars on the shear velocity and roughness estimates small. Thus, a maximum acceptable confidence band on u_* of $\pm$ 25% was chosen. This corresponds to a minimum R^2 value of 0.993. The choice of this minimum R^2 value is not without physical significance. The mean velocity profiles measured in the time period described here have regression coefficients in excess of 0.96 with one exception, and approximately 30% of those profiles have regression coefficients exceeding 0.997. The profiles with the lower regression coefficients correspond to times of observed internal wave activity penetrating to the near-bottom flow. The higher coefficients correspond to negligible internal wave activity. This result is expected when the averaging time for the mean velocity profile is short relative to the internal wave period and is discussed more below. Thus, even though all the profiles could be considered approximately logarithmic, the profiles with the lower regression values are expected to have deviations from a pure logarithmic profile that cannot be attributed to experimental error. The internal wave effects are relatively easy to observe and can be qualitatively modeled, but it is difficult to correct accurately for their effect in the present data because of their intermittent and nonlinear characteristics.

3. Results

A time series of mean flow speed and direction at 2.5 m above the bottom during a 15 h interval in CODE-1 on 2–3 June 1981, is plotted in Fig. 3. The mean flow direction changes from northward alongshelf flow, to westward cross-shelf flow, and then back to northward again. The speed decreases as the flow becomes westward and increases again as the flow returns to the north. The velocity range is from 10 to 16 cm s^{-1}.

A look at the distribution of the near-bottom kinetic energy with frequency provides a convenient description of the dynamical processes driving the flow and contributing to its variability. The low-frequency energy present between 0.002 and 0.8 cycles per minute (cpm) is illustrated in the velocity spectra in Fig. 4. The flow is forced at several discrete frequencies; a peak is evident below the semidiurnal tidal frequency (~0.0014 cpm); between tidal and Brunt-Väisälä frequencies (~0.05 cpm), several discrete peaks are evident which are an order of magnitude less energetic. Cross-spectral analysis between onshore and offshore velocity components measured by VMCM current meters at 5.5 and 7.5 m on the same mooring indicates high coherence and zero phase at these frequencies; behavior consistent with the presence of internal waves as was indicated by the temperature records.

The characteristics of the internal waves present during the time period covered by Fig. 4 are not evident from the spectral analysis. Analysis of the temporal vertical variation of individual isotherms at the top of the bottom mixed layer shows that the internal waves propagate in individual groups and are intermittently present. Typically, the groups consist of one long-period (4–5 h), large-amplitude wave with smaller-amplitude, shorter-period (1–2 h) waves following. The time period covered by the 15 h velocity record actually corresponds to three distinct time periods of internal wave

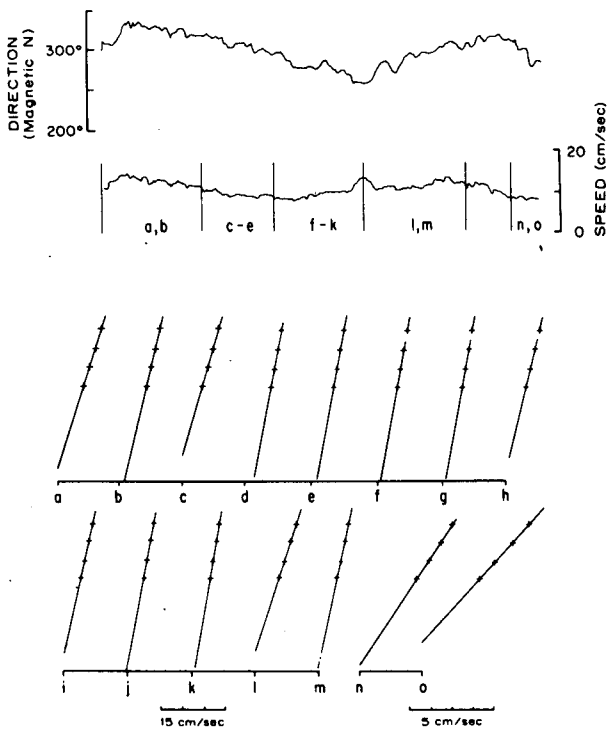

FIG. 3. Fifteen hour record of near-bottom flow at 2.5 m above the bottom at C3 (90 m of water) during CODE-1 starting approximately 2000 LST 2 June 1981. The upper plot is direction and the lower plot is speed; both are 3.33-min averages of a NBIS acoustic current meter sampled at 1 Hz. Along-isobath flow is toward 317°. The profiles are plots of logz (vertical axis) versus time-averaged (9.33 min) velocity (horizontal axis). The velocity measurements made, using the WHOI tripod system are indicated by (+) at 28, 53, 103 and 203 cm above the bottom. The straight lines represent the best-fit linear-regression line to the points. The approximate time locations of the selected profiles are indicated on the speed plot. (Note: Profiles n and o correspond to a different velocity scale).

activity; two periods (at the beginning and end of the 15 h) associated with onshelf bottom flow where the larger-amplitude internal waves propagate through the C3 midshelf site, and one period of offshelf bottom flow where the internal waves present are associated with the higher-frequency waves (smaller-amplitude waves) left over from the group of the previous onshelf flow period. The generation mechanism for these intermittent trains of internal waves is unresolved at the moment and discussion of the details of their behavior is beyond the scope of the present analysis. It is important to note only that the effect of these waves on the mean velocity profiles is not significant except near the time of maximum internal wave velocity.

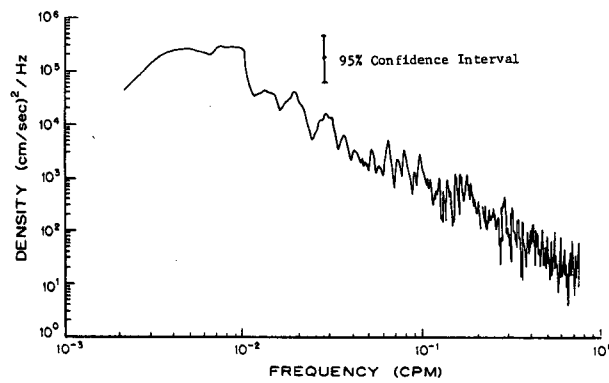

FIG. 4. Horizontal-velocity density spectra (10 degrees of freedom) from 2.5 m above the bottom for a 32-h time period including 15 hours shown in Fig. 3. The frequency scale extends from tidal to just below surface waves.

The effect of the internal waves on the mean velocity profiles is primarily kinematical resulting from unsteady effects associated with taking time averages over portions of the internal wave cycle within an internal-wave boundary layer. The energy associated with the internal wave velocities reaching the bottom is one to two orders of magnitude smaller than the energy from wind driven flows or surface waves. As a result, the maximum shear stresses from the waves are much smaller than the mean stress and the time-averaged stress contribution from the internal waves is generally insignificant (Grant, 1982). Thus, although mean velocity profiles are sometimes affected, mean stress profiles are unchanged by the internal waves. The intermittent presence of these waves is helpful in examining their effect on the mean-flow velocity profiles since profiles at time periods with and without waves can be compared with each other and with their associated stress profiles. Also, the higher-frequency waves have relatively smaller amplitudes and their velocity attenuates more quickly with depth than the earlier arriving lower-frequency waves. Thus, the higher-frequency waves have less influence on the mean velocity profiles.

The most energetic component at high frequencies in the near-bottom flow is due to long surface waves (swell). Estimates of wave direction made from velocity and pressure sensors show the swell to be propagating from a southsouthwesterly direction. Fig. 5 shows a typical spectral density for 1.2 cpm (0.02 Hz) and higher frequencies for a 20 min period during the time covered by the spectra in Fig. 4. The wave peak, at about 15 s, is narrow band and drops off to the spectral gap between the wave peak and the internal-wave band. Comparison of wave spectra over several hours indicates that the long period swell present was not stationary over time periods longer than one to two h; the peak period shifts between 14 and 18 s. Some beating is present in the swell arrival pattern at all times; a typical 10-min pressure record plotted in Fig. 6 (from the 20-min time period of Fig. 5), clearly illustrates the beat phenomena.

At frequencies above the surface wave band the velocity spectrum falls off rapidly as illustrated in Fig. 5. This trend is expected in the inertial subrange of the turbulent kinetic-energy spectrum for wavenumbers greater than approximately $2\pi/z_1$, where z_1 is the height at which the measurement is made. The vertical-

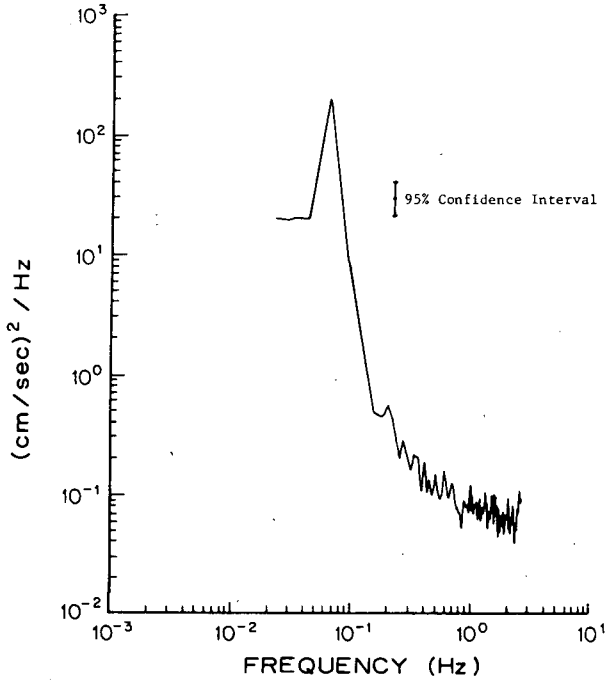

FIG. 5. Horizontal-velocity density spectra (54 degrees of freedom) showing surface wave band for a 20 min period corresponding to profiles d and e in Fig. 3. Note, over-sampling is present at high frequency because of the sensor volume averaging.

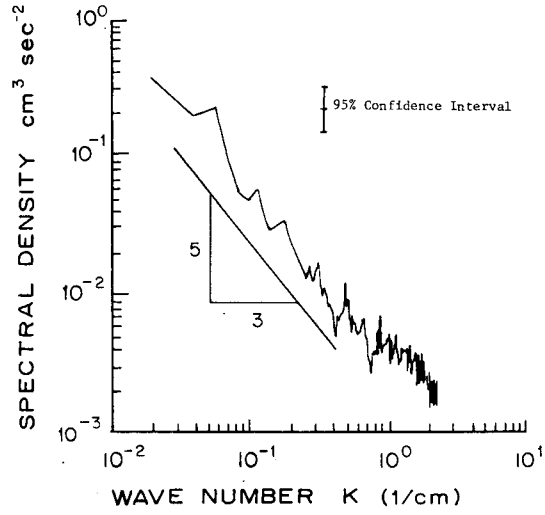

FIG. 7. Vertical-velocity density spectra (w') (54 degrees of freedom) for frequencies from surface waves into the inertial subrange. The time period corresponds to Fig. 5. The subrange spectra shows a distinct wavenumber dependence of $k^{-5/3}$ ($k = 2\pi f/u$, where u is the mean velocity). Note, oversampling at high wavenumbers corresponding to the cutoff wavenumber for the sensor averaging volume.

turbulent kinetic-energy density corresponding to Fig. 5 is plotted in Fig. 7 in terms of wavenumber. In the inertial subrange (limited to $\sim 2\pi/z_1$–$2\pi/15$ cm in Fig. 7 because of the sensor averaging volume) the slope of the density function should follow $k^{-5/3}$ from (4). The $-5/3$ line plotted in Fig. 7 agrees well with the trend in the slope of the spectrum and indicates that a well defined subrange does exist. This result will be used subsequently to examine the stress distribution.

Profiles of mean velocity averaged over 9.33 minutes, selected ($R^2 > 0.993$) from the 15-h time period are illustrated in semi-log plots in Fig. 3. Their approximate location in time is indicated on the speed plot. (Note that these profiles are chronological but do not always

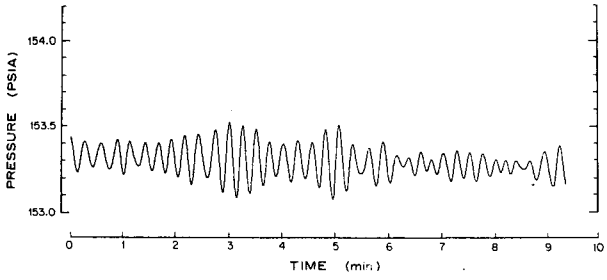

FIG. 6. Bottom pressure record (2 m above bottom) corresponding to the first 10 min of the time period in Fig. 5. The presence of a distinct beat of the long waves is evident.

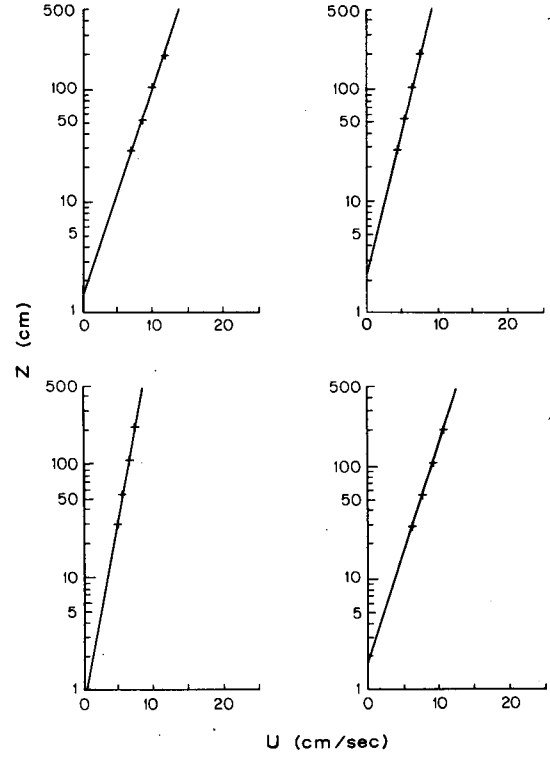

FIG. 8. Velocity profiles a, h, j and l from Fig. 3. The excellent agreement with log profiles is evident. Note, there is no consistent curvature in the profiles and the large R^2 values indicate small error bars on the u_* and z_0 estimate made from these profiles. The corresponding values of R^2, u_* and z_0 are given in Table 2.

represent back-to-back time averages). All profiles were zero-shifted downward by 2 cm. The 2 cm number was arrived at by investigating the effect of zero shifts on the fit of the velocity profiles to a logarithmic distribution. On the average, a 2 cm downward shift resulted in the maximum regression coefficient for the profiles. Four of the profiles used as typical examples are enlarged in Fig. 8. No curvature is evident in the plotted points, and the values of the regression coefficient are high. Table 2 lists values for u_*, z_0 and R^2 for all the profiles in Fig. 3. The corresponding 95% confidence limits are indicated in parentheses.

Figure 9 shows w' spectral densities at 0.5, 1.0, and 2.0 m for a typical 20 min segment (corresponding to profiles d and e) of the 15 h time period. The shear velocities calculated for each spectrum using (7) are 0.41, 0.44 and 0.48 cm s^{-1}, respectively. The shear velocities were calculated from $\phi_w(k)$ with 200 degrees of freedom. The corresponding 95-percent confidence interval on $\phi_w(k)$ is $0.83\phi_w(k) \leq \phi_w(k) \leq 1.23\phi_w(k)$. The estimates of u_* are proportional to the square root of $\phi_w(k)$, or for the 95-percent confidence interval less than a 5% uncertainty exists on estimates at each wavenumber. Over the range of wavenumbers for which estimates of u_* were calculated at each level the percent difference in u_* from the mean value was approximately ±7%. If Kolmogorov and von Karman constants are fixed, the maximum error bars on u_* are less than 10% based on statistical considerations.

The preceding estimates of shear velocity were made using the mean velocity at each level to convert frequencies to wavenumber (i.e., the frozen-turbulence hypothesis) and ignoring the effects of surface waves. The potential error due to the effects of surface waves (in the estimate of u_*) from the inertial subrange at frequencies higher than the wave peak can be roughly estimated from Lumley and Terray (1983; Appendix A). For isotropic turbulence and the horizontal wave

TABLE 2. CODE-1 BASS-W Data.

Profile	u_* (cm s^{-1})	z_0 (cm)	R^2	u_{*c}	z_{0c}	C_{D100} ($\times 10^{-3}$)	u_{100}/u_b	k_b/A_b	ϕ_c (deg)	ω (rad)
a	0.940 (±0.174)	1.46 (+1.6) (−0.77)	0.9963	0.815	0.80	9.0	1.89	0.53	30	0.459
b	0.704 (±0.107)	0.33 (+0.43) (−0.19)	0.9975	0.852	0.86	4.8	1.76	0.43	30	0.419
c	0.828 (±0.160)	2.03 (+2.11) (−1.04)	0.9960	0.704	1.0	10.2	1.46	0.46	30	0.417
d	0.580 (±0.142)	0.64 (+1.43) (−0.45)	0.9936	0.650	1.18	6.4	1.13	0.39	30	0.418
e	0.540 (±0.093)	0.72 (+0.89) (−0.40)	0.9968	0.571	0.97	6.6	1.42	0.54	30	0.426
f	0.566 (±0.134)	0.99 (+1.79) (−0.64)	0.9940	0.563	1.05	7.7	1.18	0.48	70	0.441
g	0.501 (±0.139)	0.47 (+1.49) (−0.36)	0.9920	0.562	0.94	5.8	1.35	0.55	70	0.451
h	0.674 (±0.105)	2.15 (+1.67) (−0.94)	0.9974	0.555	0.90	10.5	1.42	0.55	70	0.421
i	0.677 (±0.123)	1.91 (+1.90) (−0.95)	0.9964	0.557	0.79	9.9	1.67	0.62	70	0.423
j	0.559 (±0.111)	1.06 (+1.07) (−0.53)	0.9958	0.594	1.29	7.4	0.95	0.33	70	0.390
k	0.537 (±0.133)	0.60 (+1.45) (−0.43)	0.9934	0.603	0.98	5.9	1.29	0.46	70	0.420
l	0.915 (±0.104)	1.83 (+1.00) (−0.65)	0.9986	0.747	0.70	9.6	1.97	0.57	70	0.449
m	0.602 (±0.126)	0.89 (+1.39) (−0.54)	0.9953	0.630	1.16	7.3	1.14	0.41	30	0.425
n	0.359 (±0.090)	1.14 (+2.15) (−0.75)	0.9933	0.382	1.42	7.7	0.76	0.48	30	0.435
o	0.421 (±0.091)	1.55 (+3.02) (−1.44)	0.9950	0.431	1.52	8.6	0.73	0.40	30	0.413

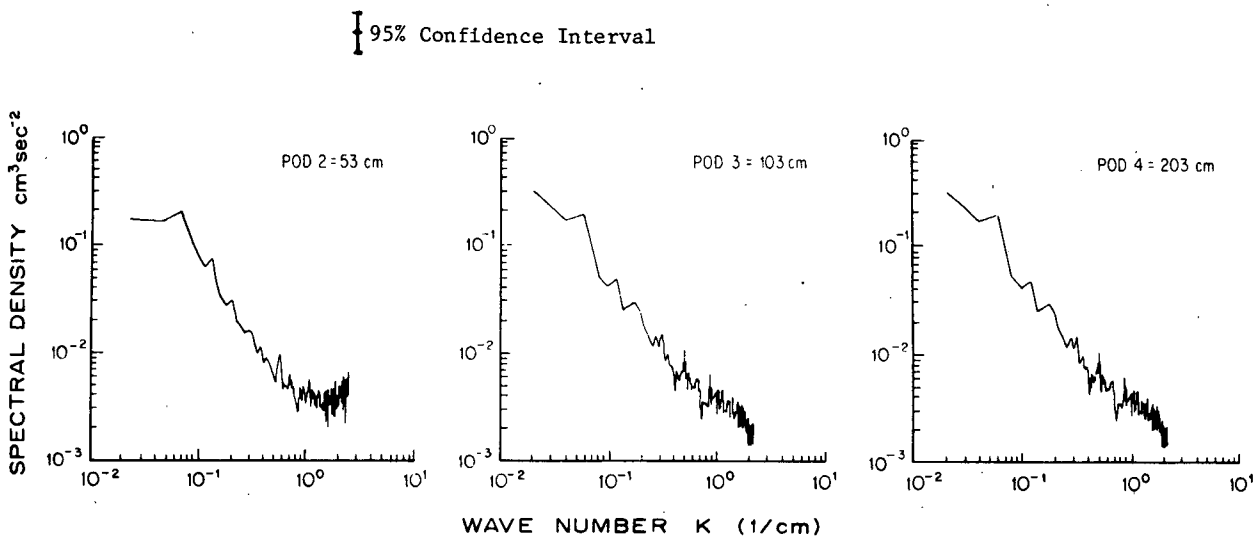

FIG. 9. Vertical-velocity spectral density showing inertial subrange for the 20.5-min time period in Fig. 10 at 53 103 and 203 cm. Each plot has 42 degrees of freedom. Wavenumbers were calculated using the Taylor hypothesis. The corresponding u_* estimates from the dissipation techniques are 0.41, 0.44, and 0.48 cm s^{-1}, respectively.

velocity much greater than the vertical wave velocity, the error is approximately $[1 - 0.1(u_{rms}/u)^2]^{1/2}u_*$, where u_{rms} is the rms horizontal orbital wave velocity and u_* is the estimated shear velocity ignoring the waves. The ratios of u_{rms}/u for the current meters at 0.5, 1.0, and 2.0 m are 0.47, 0.42 and 0.36, respectively. Using these ratios the estimated shear velocities have errors of less than 1% associated with the presence of the waves.

A second potential error in the shear velocity estimates is due to the value of the Kolmogorov constant α in (7). The range of experimental values for α appearing in the literature is close to 30% (Grant *et al.*, 1962; Champagne *et al.*, 1977; Hinze, 1975). The most dependable value for the ocean is from the work of Grant *et al.* (1962). After correcting for large wavenumber effects in the subrange, the value of α for the one-dimensional horizontal density spectrum corresponding to that of Grant *et al.* (1962) is $\alpha = 0.4$ (Hinze, 1975). For isotropic turbulence in the equilibrium range the vertical kinetic-energy spectrum is $\frac{4}{3}$ times the horizontal kinetic-energy spectrum and therefore α_3 in (7) is taken as ~0.5 for the calculations carried out here.

The shear velocity increases by 17% from the bottom to the top current meter. The variation in shear velocity over the profile is consistent with an approximate constant-stress layer when the error bars are considered.

The mean velocity profile corresponding to the same 20-min period is plotted in Fig. 10. The estimate of the shear velocity from the profile is 0.56 cm s^{-1} (±0.14 cm s^{-1} at the 95-percent confidence level). This value is not statistically different from the result from the dissipation estimates. During the 20-min time period for the results shown in Figs. 9 and 10 the internal wave activity affecting the near-bottom flow is very weak. The results for the shear velocity profiles and agreement of the estimated shear velocities from pro-

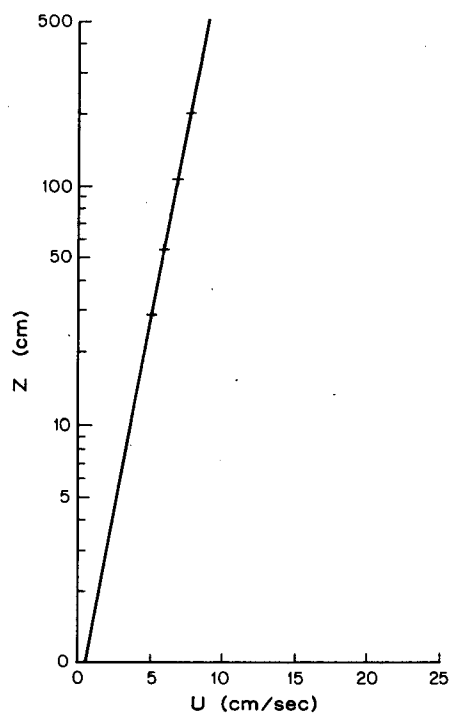

FIG. 10. Mean velocity profile (averaged over 20.5 min, covering profile d and e) for the time period covered by the power spectra plotted in Figs. 6 and 9. The values of u_* and z_0 determined from the profile are 0.566 (±0.135) cm s^{-1} and 0.65 (±1.48–0.45), respectively; $R^2 = 0.9937$.

files and dissipation techniques is typical of the entire 15-h period. During times of stronger internal wave activity, the shear velocity profiles look similar and the magnitudes of the shear velocity are in the range of the values in Table 2. Comparisons between the shear velocity estimates made using profile and dissipation techniques for the stronger internal wave cases have little meaning, however, since the confidence bands on the shear velocities from the profiles are so large.

The side-scan coverage showed that the bottom, at the tripod location, was devoid of large-scale topographic features. The sediment was a clayey–sandy silt (10% clay, 20% sand, 70% silt) and was highly bioturbated. Animal mounds and furrows from 1 to 5 cm high and densely spaced are evident in all bottom photographs. Analysis of box cores taken at the tripod locations indicates the distribution of the benthic biota to be uniform (Cacchione *et al.*, 1983).

At all times a distinct bottom mixed layer was found which varied in thickness from 15 to 30 m. The combined presence of the largest waves and lower-frequency flow resuspended very fine sediment from the bed, but threshold conditions in the usual sense were generally not exceeded. The mean concentrations of suspended sediment at 1 m were less than 2 mg l^{-1}.

4. Discussion

a. Measurements

The selected velocity profiles are described accurately by a logarithmic velocity distribution as evidenced by R^2 values greater than 0.993 and no systematic deviation of the measured points from the best fit line. This latter observation is consistent with the support data which indicate that, during the times selected, the effects on the flow structure due to stratification, internal waves and topographic features are negligible at the site. Velocity profiles were measured on one tripod for approximately 8 h of the 15 hours of data discussed here. The sampling sequence was regular with 120 min on, 60 min off, 40 min on, 40 min off, 40 min on, 40 min of. Out of the fifty-two 9.33-min profiles calculated, all but one had regression coefficients greater than 0.96 ($R^2 > 0.92$); 83% had regression coefficients greater than 0.97 ($R^2 > 0.94$) and 30% had regression values greater than 0.997 ($R^2 > 0.993$). Clearly, the profiles with R in the range 0.96–0.997 can be considered logarithmic or close to it. In our experiments a regression coefficient of 0.95 ($R^2 = 0.90$) corresponds to a 100-percent error band on u_* at a 95-percent confidence level. For the purpose of making stress and roughness estimates to be compared with model results, the fact that all of the profiles are logarithmic is of little consequence since the error bars on shear velocity determinations from those profiles with R significantly less than 0.997 are too large to make a definitive comparison.

An explanation for the range of regression values is the presence of internal waves and their effect on the averaging process to get the mean velocity profiles. The waves are well documented in the data. The bottom conditions, sediment transport, wind and near-bottom density do not change during the time period described. This is also well documented. Rather than make many assumptions required to correct the profiles for internal wave effects, we chose to make comparisons with profiles where no correction was necessary and a careful comparison of the effect of wave–current interaction could be made. The confidence band on u_*, considered as acceptable, allows comparisons with 30 percent of the measured profiles. If the acceptable band is increased to ±50% over two thirds of the profiles could be used. Such a judgment is subjective, and it was felt that more than enough data was available to make the more rigorous comparisons.

The precision of measurements of the height of the velocity sensors above the seabed is better than 1 cm with the mechanical system and O(1 mm) with the acoustic system. In spite of this relatively good precision, use of the measurement is not simple. The height of the sensor above the mean bed level around the tripod is needed. The height measurement is made at a point and therefore is affected by local microtopography (i.e., it depends whether the point is on a biologically induced mound or an indentation or slight undulation in the bottom). Pitch and roll measurements indicated no tripod settlement occurred during the analysis period. Estimates of the displacement thickness, using the results of Jackson (1981), are on the order of 1 cm and are within the uncertainty of the bottom location. The final selection of sensor height above the bottom was picked by using the zero shift, which on the average, maximized the regression fit of the logarithmic profiles to the actual measured velocity points. A 2-cm downward shift was used. It is noteworthy that 2 cm is equal to the uncertainty in the mechanical system plus the displacement height. Overall, zero shifts in the mean bottom location affected the confidence levels most and had only a minor effect on the estimates of z_0 and u_* based on the velocity profiles since the velocity measurements were mostly above the region of maximum shear.

Averaging time intervals between 9 and 14 min consistently gave the highest R values. Other averaging intervals of 4.67 and 18.67 min yielded very similar results for u_*, but in general, increased the scatter in z_0 and decreased the regression coefficients slightly. Averaging times less than 4.67 min significantly lowered the regression coefficients and increased the scatter in both u_* and z_0.

It is well established that the existence of logarithmic profiles requires averaging the instantaneous velocity over a long enough interval to properly average the eddy structure in the flow (Townsend, 1970). The lower limit on the time averages requires that the averaging

time must be sufficiently greater than the eddy-mixing time scale z/u_*. For the CODE site in the lower 2 m this is at least 4 or 5 min [$z/u_* \sim O(10^2)$ s]. However, the beat period of the surface waves is on the order of two minutes and averages over several periods are needed. This means that a minimum averaging time of close to 10 minutes is desirable. Thus, some degradation of the velocity profiles at averaging times much less than 10 minutes is expected. As the averaging interval is increased, effects of nonstationarity and unsteadiness in the flow field become important. The variability in the bottom velocity profiles due to intermittent internal waves with frequencies of 10^{-2} cpm and lower, although weak, could still be picked out. Averaging intervals must be kept small, relative to internal wave variability and this generally limited averages to 30 minutes or less. It was not possible to average over longer times to remove internal wave effects because the system is not stationary at these longer time scales as evidenced by the swell behavior and variability in the bottom currents (Fig. 2). The choice of an averaging interval of approximately 10 minutes maximized the regression coefficient in most cases.

The net result from the choice of zero shifts and averaging times is to maximize the value of the regression coefficients for the profiles and minimize the error bars on the estimates of u_*, z_0 and the velocity profiles. The 95-percent confidence intervals on the estimates are included in Table 2. The intervals on u_* are always less than ±25% and as low as ±10%.

The shear velocity estimates based on the inertial dissipation technique and the velocity profile technique (Figs. 9 and 10) agree within statistical limits. Furthermore, the shear velocity estimates at all three levels show approximate agreement within their error bars. The picture is consistent with an approximately constant stress layer and the corresponding existence of a logarithmic velocity profile. It is well known that a constant stress layer is not required over the entire region that the logarithmic velocity profile is observed to exist (e.g., Tennekes, 1973; Hinze, 1975). It is only in the asymptotic sense as the boundary is approached that the stress should be constant. Typically, the log layer is expected to be approximately 10 percent of the boundary-layer thickness. For the flow conditions here the log layer should be approximately 3.5–4.0 m thick and hence the lower 2 m should be expected to approach a constant stress layer as observed.

During time periods when the velocity profiles cannot be used to estimate the shear velocity with the desired accuracy, the dissipation technique can be used instead. This technique cannot be used to estimate roughness length without some assumptions on the relationship between roughness and stress, however. The usual choice would be that the profiles are logarithmic. This reverts the problem to making the internal wave corrections to the profiles or accepting large confidence limits on the estimates. Thus, no discussion of the results is given for time periods when the profiles are not within stated limits, other than to state that the shear velocity values are typical of the large values observed in the profile estimates.

The results of analysis indicate that velocity profiles can be used to estimate stress with very specific limitations. The first limitation is that the fit of the velocity profile to a logarithmic distribution must be sufficiently good (as measured by the regression coefficient and curvature in the profile) that the stress is within some preset error bars. The second limitation is the averaging time as discussed above. Spectra by themselves do not indicate the appropriate time averaging interval sufficiently and a careful analysis of the time series of events is important. The third major limitation is the knowledge of the bed origin. It is important to have some method to set limits on zero shifts in the velocity profiles. Even a bottom locator at a single point must be interpreted with care.

The profiles exhibit large values of z_0 and u_* relative to those typically expected for a quasi-steady flow over a relatively uniform bottom. For the velocities observed at 1 m, the corresponding drag coefficients C_D range from 5×10^{-3} to 11×10^{-3} (based on $\tau_c = \rho C_D|\mathbf{u}|\mathbf{u}$). These values are approximately 3 to 7 times larger than the number $\sim 1.5 \times 10^{-3}$ that many modelers (Allen, 1980; Brink and Allen, 1978; Brink, 1982) use for the shelf and clearly are not constant. The drag coefficient will vary with the height of the reference velocity so comparing values used by various investigators is difficult (e.g., Winant and Beardsley, 1979). The value of 1.5×10^{-3} corresponds to a smooth bottom. In fact, the bottom at the site would be expected to be smooth, given the sediment type and the flow conditions, except for the biological effects. A more realistic value of 3×10^{-3} corresponding to the *observed* physical bottom roughness is still well below the C_D values observed. The range of z_0 values of 0.3 to 1.9 cm is large for the bioturbated bottom carefully observed in bottom photographs and box core surfaces; an estimate of the physical z_0 for these features is ~0.1 cm; nearly an order of magnitude smaller than estimated from the majority of the profiles (Table 2).

To emphasize further the size of the u_* and z_0 values observed, typical drag coefficients and roughness heights from a time period during CODE-2 at the same site are given in Table 3. (The values were estimated using the profile technique.) During the period to which these values correspond, the mean currents were much stronger than the surface wave velocities as indicated by the u_{100}/u_b values for each profile. The z_0 values are near 0.1 cm and the drag coefficients near 3×10^{-3}. The bottom at the site is similar to its configuration during CODE-1 (i.e., bioturbated mounds and furrows) and the value of z_0 near 0.1 cm is expected. (This is discussed later under comparison with theory.) The values given in Table 3 are from two

TABLE 3. CODE-2 deployments.

	u_{100}/u_b†	z_0 (cm)#	u_* (cm/s^{-1})	C_D ($\times 10^{-3}$)	R
a*	3.85	0.095	1.13	3.3	0.9971
b	3.57	0.184	0.90	3.9	0.9989
c	4.35	0.284	0.96	4.4	0.9970

No zero shift has been applied to these profiles so the adjusted values will be slightly smaller than given.

* b and c are from one tripod; a is from a second tripod deployed nearby. The values given here are close to the same time period but do not overlap.

† Time averages are for 10 min; u_b is the maximum orbital wave velocity over the 10-min period.

different tripods deployed within a kilometer of each other during approximately the same time period. (The flow conditions to which these values correspond were anomalous during both CODE-1 and CODE-2 and will be discussed in a future publication.)

Control in the experiment is good and the support data justify the neglect of effects associated with internal waves, stratification and large-scale upstream topography. The type of stress behavior observed during the 15-h period discussed is qualitatively expected based on the combined wave and current models developed by Grant and Madsen (1979) and Smith (1977). The measurements of velocity were made outside the wave boundary layer region where enhancement of the mean stress and apparent roughness are predicted to occur. (Estimates of the wave boundary-layer thickness are made later to show that this is the case). We demonstrate in the next section that interaction between the low-frequency currents and surface waves provides a dynamical explanation for the observed shear velocity and roughness values.

b. *Comparison with combined wave and current models*

1) THEORETICAL MODEL

The physical situation treated by the combined wave and current models is described by Grant and Madsen (1979) and briefly summarized here. As derived below, unsteady boundary layers have thicknesses which scale as $\kappa u_*/\sigma$, where u_* and σ are the characteristic shear velocities and frequencies. Thus, because of the contrasting time scales associated with the combined wave and current flow, two distinct bottom boundary layer regions develop. A wave boundary layer develops in the immediate vicinity of the boundary, its growth being limited by its short time scale to several centimeters for the flow characteristics in the experiments. The wave boundary layer is nested within a thicker current boundary layer where thickness is limited by the local inertial frequency. This current boundary layer develops well away from the boundary up to 20 to 40 m in height for the flow conditions at CODE. Within the wave boundary layer, the turbulence intensities are due to the combined flow which is coupled in a nonlinear manner. Above the wave boundary layer (i.e., in the potential flow region for the wave), the turbulence is associated only with the low-frequency "mean" flow. This mean flow is altered, however, because of the flow momentum removed below by the action of the combined shear flow. The result is that the current above the wave boundary layer experiences a shear stress dependent on the wave boundary-layer characteristics as well as on the physical boundary characteristics, i.e., animal mounds, ripples, etc.

Mathematically, we describe the near-bottom fluid motion in both regions, neglecting nonlinear and Coriolis terms, as

$$\frac{\partial \mathbf{u}}{\partial t} = -\frac{1}{\rho}\nabla_H p + \frac{\partial}{\partial z}\left(\frac{\tau}{\rho}\right), \tag{11}$$

where τ is the bottom stress, t is the time, ∇_H is the horizontal vector operator

$$\nabla_H = \frac{\partial}{\partial x}\mathbf{i} + \frac{\partial}{\partial y}\mathbf{j}, \tag{12}$$

p is the pressure

$$p = p_w + p_c \tag{13}$$

and u is the velocity vector

$$\mathbf{u} = \mathbf{u}_w + \mathbf{u}_c, \tag{14}$$

where the subscripts w and c indicate the components due to the wave and current.

In the Grant and Madsen (1979) model, turbulence closure for (11) is made through a linearly varying eddy viscosity given by

$$\nu_T = \kappa u_* z, \tag{15}$$

where u_* is the characteristic shear velocity for the flow. Eq. (15) is a useful approximation to the full eddy viscosity profile given approximately by $\kappa u_* z e^{-z/h}$ where h is the boundary-layer scale height (e.g., Long, 1981; Glenn, 1983; Grant and Glenn, 1983) and permits analytic solutions to be found to (11).

Since two distinct boundary layers exist for the flow, a characteristic shear velocity for each region must be determined. These shear velocities are found using the definition of the instantaneous boundary shear stress

$$\tau_b = \frac{1}{2}\rho f_{cw}(u^2 + v^2)^{1/2}[u, v], \tag{16}$$

where f_{cw} is a wave–current friction factor, and u and v are the x and y components of the instantaneous horizontal velocity. Adopting the convention that the x-axis is always in the direction of wave propagation, u and v are

$$u = \left(\sin\theta + \frac{|\mathbf{u}_a|}{|\mathbf{u}_b|}\cos\phi_c\right)|\mathbf{u}_b|, \tag{17}$$

$$v = \left(\frac{|\mathbf{u}_a|}{|\mathbf{u}_b|}\right) \sin\phi_c |\mathbf{u}_b|, \tag{18}$$

where $|\mathbf{u}_a|$ is the magnitude of the steady current velocity at a height a above the bed, ϕ_c the angle made by $|\mathbf{u}_a|$ with the direction of wave propagation, $|\mathbf{u}_b|$ the maximum near-bottom orbital wave velocity from linear wave theory

$$|\mathbf{u}_b| = \frac{H}{2\sinh kh}\omega \tag{19}$$

in which H is the wave height, k the wavenumber, h the water depth and ω is the radian wave frequency and $\theta = \omega t$ is the phase angle for the wave.

In the region above the wave boundary layer, i.e., the potential flow region for the wave, the stress is associated with only the mean flow and the current above feels the time-averaged stress. The instantaneous flow is continually changing direction, and (16) is time averaged with respect to direction to define the mean shear velocity in the outer region, $|\mathbf{u}_{*c}|$. Inside the wave boundary layer the majority of turbulence production occurs during the maximum wave velocity and the characteristic shear stress for this region is argued to be the maximum, $|\mathbf{u}_{*cw}|$. Note that the use of $|\mathbf{u}_{*cw}|$ in (15) means that the eddy viscosity is time-independent. In addition to the physical reasons stated, Trowbridge (1983) has demonstrated that to first order the time variation may be neglected in a fully time-dependent eddy-viscosity model.

The respective wave and current velocity profiles are found by solving (11) in each boundary layer region using the proper shear velocity for each region as defined above. From the governing equation for the wave motion within the wave boundary layer it is easily shown that the vertical scale of the oscillatory boundary layer is

$$l = \frac{\kappa|\mathbf{u}_{*cw}|}{\omega}. \tag{20}$$

The primary interest here is in solutions for only the mean flow in the outer boundary layer region. To solve for the steady component of (11), the usual boundary layer assumption is applied and a constant stress region is assumed to exist in each layer. Within the wave boundary layer the usual no-slip boundary condition is

$$\mathbf{u} = 0 \quad \text{at} \quad z = z_0, \tag{21}$$

where z_0 is the physical bottom roughness length; i.e., the roughness scale associated with bedforms, ripples or animal mounds, for example. The resulting velocity profile in this region (Grant and Madsen, 1979) is

$$|\mathbf{u}| = \frac{|\mathbf{u}_{*c}|}{\kappa}\frac{|\mathbf{u}_{*c}|}{|\mathbf{u}_{*cw}|}\ln\frac{z}{z_0}, \quad z < \delta_w, \tag{22}$$

where δ_w is the wave boundary-layer thickness.

For the flow above the wave boundary layer the no-slip condition is taken as

$$\mathbf{u} = 0 \quad \text{at} \quad z = z_{0c}, \tag{23}$$

where z_{0c} is the apparent roughness that reflects the influence of both the physical bottom roughness and the dissipation associated with the wave generated turbulence.

Using the condition in (23) the solution for the mean flow above the wave boundary layer is

$$|\mathbf{u}| = \frac{|\mathbf{u}_{*c}|}{\kappa}\ln\frac{z}{z_{0c}}, \quad z > \delta_w. \tag{24}$$

The relation between the two roughness lengths z_0 and z_{0c} is determined by matching the velocity profiles across the boundary layer interface. Equating (22) and (24) at $z = 2l$ (Eq. 20), the ratio between the apparent roughness and physical bottom roughness is

$$\frac{z_{0c}}{z_0} = 24\left(\frac{|\mathbf{u}_{*cw}|}{|\mathbf{u}_b|}\frac{|\mathbf{A}_b|}{k_b}\right)^{\beta}, \tag{25}$$

$$\beta = \left(1 - \frac{|\mathbf{u}_{*c}|}{|\mathbf{u}_b|}\frac{|\mathbf{u}_b|}{|\mathbf{u}_{*cw}|}\right), \tag{26}$$

where k_b is the equivalent roughness height equal to $30z_0$ for rough turbulent flow and $|\mathbf{A}_b|$ is particle excursion amplitude $= |\mathbf{u}_b|\omega^{-1}$.

Grant and Madsen (1979) define the wave boundary-layer thickness as $\delta_w = 2l$, where l is given by (20). With this definition (25) can be rewritten for rough turbulent flow as

$$\frac{z_{0c}}{z_0} = 24^{1-\beta}\left(\frac{\delta_w}{z_0}\right)^{\beta}. \tag{27}$$

Thus, (27) illustrates that the apparent roughness depends on the relative turbulent intensity within the wave boundary layer and the wave boundary-layer thickness as well as the physical bottom roughness.

To apply the model summarized above, the wave friction factor and the apparent roughness must be determined. These are solved for in the model as a function of four parameters characterizing the near-bottom flow. In dimensionless form these four parameters are (Grant and Madsen, 1979)

$$\frac{z_r}{k_b}, \quad \frac{|\mathbf{u}_{cr}|}{|\mathbf{u}_b|}, \quad \frac{k_b}{|\mathbf{A}_b|}, \quad \bar{\phi}_c, \tag{28}$$

where $|\mathbf{u}_{cr}|$ is the magnitude of the mean velocity at a height z_r above the bed, $\bar{\phi}_c$ the angle between the wave and current and $|\mathbf{u}_b|$ and $|\mathbf{A}_b|$ characterize the wave; and k_b is the physical bottom roughness ($k_b = 30z_0$). The iterative procedure used to calculate the stress, apparent roughness and velocity profile is described by Grant and Madsen (1979).[4] (Note, if sediment

[4] There is a typographical error in Eq. (54) of Grant and Madsen (1979): $\alpha^{3/4}/4$ should be $\alpha^{3/2}/4$.

transport is occurring, z_0 is a function of the shear stress and must be calculated iteratively as described by Grant and Madsen, 1982, or Grant and Glenn, 1983).

2) COMPARISON WITH CODE-1 RESULTS

The CODE dataset contains all the necessary information to calculate the four parameters in (28). For the conditions observed during the experiments, the wave boundary layer is 1 to 4 cm thick and is well below the measurement region of the lowest current meter located at approximately 30 cm above the bottom. Thus, according to the model the velocity profiles measured in CODE-1 correspond to the solution given by (24); the calculated roughness lengths correspond to the apparent roughnesses z_{0c}, and the calculated shear velocities u_{*c} correspond to the mean shear stress enhanced by the presence of the waves.

At the C3 station, bottom photographs and box cores show that the bed features are mounds and furrows created by benthic biota; they range in height from 1–5 cm and are spaced on the order of 10–30 cm apart (Cacchione *et al.*, 1983). The height-to-width dimensions are nearly one-to-one. The available information on estimating roughness lengths for three-dimensionally distributed roughness elements is sparse and even for uniformly distributed roughness elements the empirical approaches available are based on only limited data. We based our estimates on the approach of Wooding, *et al.* (1973) where the roughness length k_b is proportional to the roughness element height k, its concentration λ, and a three-dimensional factor ϕ. Thus,

$$k_b \propto k\lambda\phi \tag{29}$$

where λ is the ratio of the frontal area to the average area of the flat surface occupied by the roughness element, and ϕ is proportional to the ratio of the height of the roughness element to its width, raised to an empirically determined power.

Grant and Madsen (1982) have demonstrated that (29) holds well for ripples in oscillatory flow with ϕ taken as one and the proportionality constant between k_b and λ equal to approximately 30. Most recently, Paola (1983) has carried out steady flow laboratory experiments over uniformly placed hemispheres corresponding to the concentration-dependent roughness range where (29) should be valid. Experiments were also run with downstream tails on the hemisphere to investigate three-dimensional flow effects. In all cases Paola found that k_b was scaled best by a $k\lambda$ distribution.

Based on the seabed geometry and (29), an order-of-magnitude estimate for k_b at the site is $30k^2L^{-1}$, where L is the spacing of the mounds. Substituting typical numbers gives $z_0 = k_b/30 = O(10^{-1})$ cm. The flow conditions during the experiments were not sufficient to cause much sediment transport at the bed. Thus, the major contribution to the roughness should be expected to be from the animal mounds. Moreover, this roughness should stay constant during the course of the measurements because of the minimal amount of sediment transport.

The values for z_0 given in Table 3 for the relatively small wave-to-current velocity ratios correspond approximately to the physical bottom roughness since wave–current interaction is not expected to be significant at these small relative wave velocities. The measurements were taken during CODE-2, but for the same time of year and at the same site. Bottom photographs and box cores indicate that the bottom conditions are similar in CODE-1 and CODE-2. The analysis of these CODE-2 profiles still requires refinement, which may result in as much as a 15% difference in the z_0 values, but the values indicate that estimates of the physical roughness of magnitude 0.1 cm are quite reasonable.

Characteristic wave velocities and periods were determined from the data for use in the model through the parameters, $|\mathbf{u}_{cr}||\mathbf{u}_b|^{-1}$ and $k_b|\mathbf{A}_b|^{-1}$, in (28). The mean flow was determined from averages over time periods of approximately 10 min. During any 10-min time period there is variability in the surface waves as is obvious from the beating in Fig. 6. The largest contribution to wave-induced turbulence during the time period over which the current is averaged will be associated with the largest waves. The enhancement of mean stress associated with the effect of surface waves is a highly nonlinear process also weighted toward the largest waves. In addition, the apparent roughness is proportional to the total stress and the thickness of the wave boundary layer as seen from (27).

Two possible choices for the wave description are then the maximum wave characteristics or the significant wave characteristics. Examination of the wave patterns, such as the one plotted in Fig. 6, indicates that the envelopes describing the waves are generally quite flat and the maximum and significant wave heights are not greatly different. The period also shows relatively little scatter. Thus, as a convenient choice in this dataset, we characterize the waves by the amplitude of the envelope of the wave record over the mean-flow averaging period and use the average wave period during this time.

To estimate the variability in the results of the model run due to the choice of statistics to represent the wave, we undertook a wave-by-wave analysis of several time series. The mean current over a given 10-min interval was held constant. From the pressure record, the wave velocity and period were calculated for each individual wave over the same 10-min period. The model was then run for each wave, and $|\mathbf{u}_{*c}|$ and z_{0c} were determined for the average of the individual runs. Comparison of this wave-by-wave result with the result using the beat envelope amplitude and average period showed only a 10–12% difference in $|\mathbf{u}_{*c}|$ estimates and a 20–40% difference in z_{0c}. These numbers are well within

the error bars on the respective estimates made from the velocity profiles; thus, the choice of the more easily calculated statistics is used here.

The combined wave and current model was run for the CODE data using as inputs the mean velocity at 1 m, the wave velocity based on the maximum envelope amplitude and the average wave period over the time corresponding to the current-averaging interval, the average direction between the wave and the current and an estimated value for the physical bottom roughness of 0.1 cm. The value of the physical bottom roughness was then adjusted in increments of 0.1 cm until a good fit between the model predictions of $|\mathbf{u}_{*c}|$ and estimates from the data were obtained for the first two profiles. We found that the predictions of $|\mathbf{u}_{*c}|$ were not highly dependent on the roughness estimates; a correction of 0.1 cm typically changed the difference between predicted and estimated values by no more than 12–15%. A value of z_0 equal to 0.2 cm (or $k_b = 6$ cm) was picked and held constant throughout the entire 15-h period shown in Fig. 3. This value is consistent with the estimates of the magnitude of roughness given before since the result given by (29) only provides an order of magnitude for z_0 in the case of distributed roughness elements.

The estimated values of $|\mathbf{u}_{*c}|$ and those predicted by the model are plotted in Fig. 11. The error bars on the estimates are also indicated. In general, the predictability of the $|\mathbf{u}_{*c}|$ values can be done within 10–15 percent and within the error bars on the estimates from the measurements. Fig. 11 also indicates the comparison between predicted and estimated values of the apparent roughness. The estimates of the roughness lengths based on the data are inherently noisy; in spite of this, the model predictions and estimates are in good agreement.

Differences in the predicted values of $|\mathbf{u}_{*c}|$ and z_{0c} result from the use of a two-piece linearly varying eddy viscosity given by (15) as opposed to the full exponential form or a continuous approximation of it. Use of (15) requires an assumption on the magnitude of the wave boundary-layer thickness since the velocity profiles in each boundary layer region must be matched. The value is taken as $2l$. This value has limited support from comparisons of the theory in the limiting case of a pure wave motion with laboratory data (Grant, 1977). Boundary layer thickness varies depending on whether the definition is based on a fixed percentage of the free stream velocity or of the bottom stress, for example. In reality there is a gradual transition of stress, momentum flux and kinetic energy as one moves from the region dominated by wave-induced turbulence to that dominated by mean flow-induced turbulence. An exact boundary layer definition is impossible to prescribe. The sensitivity of the combined wave and current model to the boundary layer definition has been demonstrated to be weak (Grant, 1977).

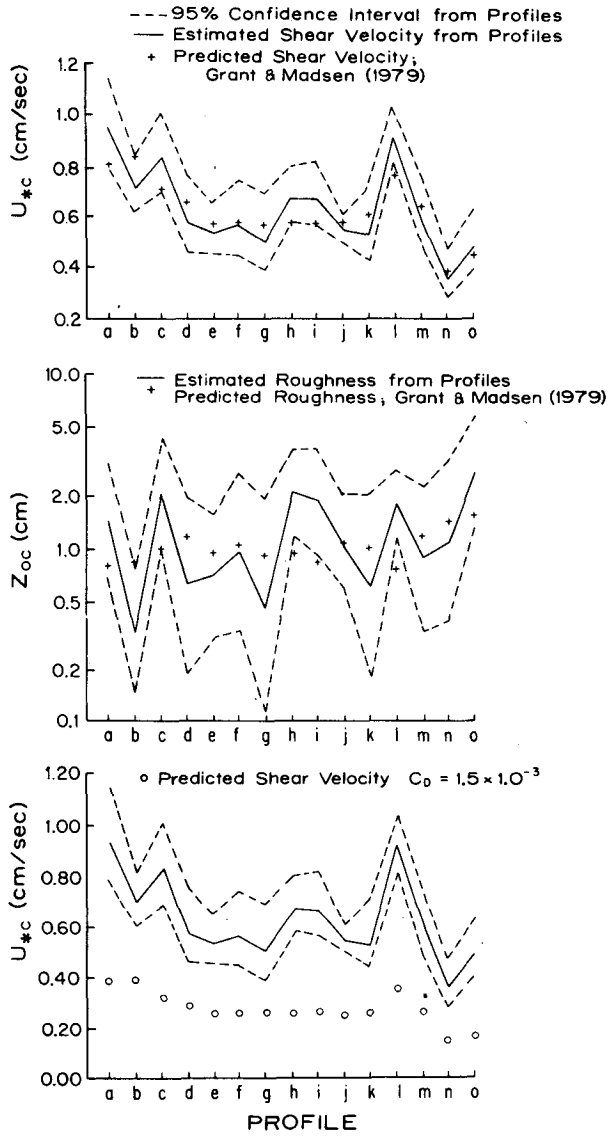

FIG. 11. CODE-1 data-model comparison, shear velocity and bottom roughness estimated from measured velocity profiles and predicted by the neutral near-bottom model. Also shown is the shear velocity calculated with the smooth bottom-drag coefficient $C_D = 1.5 \times 10^{-3}$.

A kink results in the velocity profiles at the interface between the wave boundary-layer region and the outer boundary-layer region as a consequence of the use of the two-piece linearly varying eddy viscosity. The use of a continuous eddy viscosity results in a smooth transition between the boundary layers. Above and below the transition, the log profiles given by (24) and (22), respectively, are good approximations to the continuous velocity profiles. Comparison between the Grant and Madsen (1979) model and a full eddy viscosity model (Glenn, 1983) demonstrate that differences in estimates of u_* are minor, less than 20 percent. For the purposes of predicting the near-bottom flow

and the mean stress, considering the other sources of variability such as bottom roughness and the assumptions in the full eddy viscosity model, the linearly varying model is sufficiently accurate, and the analytical solutions that it allows make it convenient to use.

The stress estimates are only slightly sensitive to the angle between the wave and the current, when the angles are less than 45 deg, as predicted by the model. An improvement of less than 10 percent in prediction of $|\mathbf{u}_{*_c}|$ occurs by including direction for the range of CODE values. The magnitudes of the values estimated for the physical bottom roughness using (28), are argued to be reasonable through existing laboratory evidence from recent work by Grant and Madsen (1982) in oscillatory flow and from the CODE-2 experiments such as shown in Table 3. Changes in the estimates of the physical bottom roughness of any reasonable number can not explain the roughness values observed in the data. The *physical* roughness value used in the model runs was kept constant for all the runs (for reasons argued before) and we were able to predict the variation in the *apparent* roughness values estimated from the data; more evidence for the reasonable estimate of the physical roughness.

In CODE-1 a second tripod was deployed simultaneously within 500 m of the tripod on which the measurements described here were made. The same results were found to hold for this second tripod. An even more detailed follow-up experiment (CODE-2) was carried out at the same site in the spring of 1982. Similar results have been found from initial data analysis except for the anomalous time described in Table 3. Results from the same multi-tripod deployment schemes as were used in CODE-1 are again consistent for all runs examined to date.

Shelf modelers have generally used bottom friction models based upon constant drag coefficients. The usual number employed on the shelf for a fine sediment bottom such as CODE is approximately $C_D = 1.5 \times 10^{-3}$ (where $\tau_b = \rho C_D|\mathbf{u}|\mathbf{u}$) as pointed out previously. Fig. 11 compares the shear velocity estimated using the constant drag coefficient referenced to the velocity 1 m above the bottom with the shear velocity values from the profiles discussed here. It is important to note that the *apparent* qualitative correspondence between the shear velocity estimates from the conventional drag estimate and the data is simply a consequence of the fact that during the 15-h period plotted the relative strength of the waves and currents did not vary greatly. Therefore, the underlying trend of the temporal variability in the shear velocity, which is caused by the current, will be similar in the drag coefficient parameterization and the wave–current model as shown in Fig. 11. The values for C_D in Table 2 demonstrate that as the relative strength of the waves and currents changes, the actual value of C_D can change considerably. The values for C_D in Table 3 show the result of an extreme change in the relative wave and current conditions which can be compared to the small changes during the 15-h period described in this paper. Other time periods of different relative wave and current activity during CODE-1 give different apparent drag coefficients. During the 15-hour CODE-1 time period, the values of the drag coefficient calculated from the measurements are 3–7 and 1.5–3.5 times larger than the constant smooth-bottom or rough-bottom values of 1.5×10^{-3} and 3×10^{-3}, respectively, for the *relatively mild wave* conditions observed.

5. Summary and conclusions

High quality bottom boundary-layer measurements from CODE-1 have been analyzed for velocity profiles, roughness lengths and shear stress estimates. Data from typical spring and early summer flows were examined. The results of the analysis were compared with predictions of Grant and Madsen's (1979) combined wave and current model. The analysis and comparison show:

- The mean velocity profiles can usually be classified as logarithmic as would be expected for flow over the simple relatively flat bottom at the CODE site. The deviations from logarithmic mean profiles that occur can be generally attributed to the effects of unsteadiness induced in the averaging process by the presence of weak internal wave velocities. This effect of the internal waves is argued to be kinematical and does not affect the true form of the mean velocity profile or bottom stress.
- Shear velocity estimates based on inertial dissipation estimates made from the power spectra indicate approximately a constant stress layer in the lower 2 m; a result consistent with the log profiles found.
- Shear velocity and roughness estimates were made from velocity profiles free from significant internal wave effects ($R^2 > 0.993$) which resulted in 95-percent confidence bands of ±25% or better on u_* estimates. The roughness length and shear velocity value estimates are much larger than can be explained by the physical bottom roughness and mean flow alone ($u_* \sim 0.5$–1.0 cm s^{-1}, $z_0 \sim 1$ cm). Support data on temperature and salinity, suspended sediment, large-scale topographic feature and internal waves demonstrates that the observed u_* and z_0 values cannot be attributed to their influence.
- The remaining explanation for the value of the estimates is surface waves. Comparisons between data estimates and predictions using the combined wave and current model of Grant and Madsen (1979) show good agreement between estimated and predicted u_* and z_0 values.
- A minor problem with the prediction scheme is the estimation of the physical bottom roughness over a bioturbated bottom characteristic of the midshelf region of the CODE site. Although we can estimate the order of magnitude of the physical bottom roughness, the actual values must be determined empirically.

This does not affect the validity of the results, but does complicate predictions unless bottom photographs or box cores are present.

- The data and model show that using the constant drag coefficient approach for a smooth bottom ($C_D \sim 1.5 \times 10^{-3}$) results in under-prediction of bottom stress and fails to reproduce the variability in the stress. Improvement in the magnitude prediction occurs when the bottom roughness is considered ($C_D \sim 3.0 \times 10^{-3}$) but the stress is still underpredicted significantly. Both stress values are outside the 95-percent confidence limits on the data estimates.

The wave and current conditions observed at the CODE-1 site are typical for spring and early summer along the west coast shelf, north of San Francisco. Analysis of year-long records for the coastal-wave data network indicates the presence of long ocean swell during most months of the year. Swell with periods of 12 s or greater reaches bottom over most of the shelf. The effects of the waves on near-bottom current profile and stress predictions was pronounced even for the gentle wave signal present. Measurements in CODE-2 with stronger relative mean flows still indicate a pronounced wave effect until an upper limit is reached where the waves have no significant effect on the mean flow. Future analysis will resolve the upper limit. Additional measurements from a winter storm (Grant *et al.*, 1983) in the CODE region, with much larger relative values of waves to currents, demonstrate an even more pronounced wave effect and show good comparison with the Grant and Madsen (1979) and (1982) theories.

The stress values presented are estimates and their accuracy is dependent on the method used to make the estimates. The correspondence between the estimates from the dissipation and profile techniques is a good measure of the quality of the dataset. The estimates of stress from the data and the model predictions compared to them were only for the mean bottom stress influencing the mean velocity profile above the wave boundary layer. This number is crucial to determining the mean friction on the shelf for shelf-circulation modeling. It is important to sediment transport calculations in that it controls the mean flow transporting the sediment over most of the bottom boundary layer. It must be emphasized, however, that the instantaneous stress acting inside the wave boundary layer, 1–10 cm thick, is responsible for resuspension of the sediment from the bed. We do not measure this stress value directly in the field nor do we discuss it here (the instantaneous stress is calculated in the wave–current model). The point is that care must be used when interpreting and applying stress values estimated in the field.

The results reported here allow us to make accurate predictions of the mean bottom stress from knowledge of the surface wave climate, water density profile, the bottom characteristics and the current at some level within the bottom boundary layer. An important caveat is that the local topography influencing the current must be simple. This is the case at the CODE mooring sites. The results presented here along with the field measurements of Cacchione and Drake (1982), Butman *et al.* (1979), Forristall *et al.* (1977) and Grant *et al.* (1983) provide strong support for the general importance of wave–current interaction to bottom stress behavior and boundary layer processes on continental shelves.

Acknowledgments. The data presented and analyzed here were taken as part of the Coastal Ocean Dynamics Experiment (CODE) Bottom Boundary Layer and Shear Stress Component under the National Science Foundation Sponsorship Grant OCE-8014938. P. Dragos did much of the programming for the data analysis. J. Newman, C. Pilskaln and L. Sanford contributed significantly to the data analysis. C. Dunn provided critical field support. D. Cacchione, D. Drake and other USGS personnel provided critical collaboration on the experiments. The crew and Captain of the R.V. *Wecoma* provided excellent field support. Supporting data and results and reviews were provided by several CODE P.I.s. B. Pratt did the graphics. We thank all these people for their assistance. G. McManamin typed the manuscript for which we express our appreciation.

REFERENCES

Allen, J. S., 1980: Models of wind driven currents on the continental shelf. *Annual Reviews of Fluid Mechanics,* Vol. 12, Annual Reviews, 389–433.

——, R. C. Beardsley, W. S. Brown, D. A. Cacchione, R. E. Davis, D. E. Drake, C. Friehe, W. D. Grant, A. Huyer, J. D. Irish, M. M. Janopaul, A. J. Williams and C. D. Winant, 1982: A preliminary description of the CODE-1 field program, *CODE Tech. Report No. 9,* WHOI Tech. Rep. No. 82-51, 47 pp.

Bakker, W. T., and Th. van Doorn, 1978: Near-bottom velocities in waves with a current. *15th Coastal Engr. Conf.,* pp. 1394–1413.

Brink, K. H., 1982: "The effect of bottom friction on low-frequency coastal trapped waves. *J. of Phys. Oceanogr.,* **12,** 127–133.

——, and J. S. Allen, 1978: On the effect of bottom friction on barotropic motion over the continental shelf. *J. Phys. Oceanogr.,* **8,** 919–922.

Butman, B., M. Noble and D. W. Folger, 1979: Observations of bottom current and bottom sediment movement on the mid-Atlantic continental shelf, (abstract). *J. Geophys. Res.,* **84,** 1187–1205.

Cacchione, D. A., and D. E. Drake, 1979: A new instrumentation system to investigate sediment dynamics on continental shelves. *Mar. Geol.,* **30,** 299–312.

——, and ——, 1982: Measurements of storm generated bottom stresses on the continental shelf. *J. Geophys. Res.,* **87,** 1952–1961.

——, ——, W. D. Grant and A. J. Williams, III, 1983: Variability of Sea-Floor roughness within the Coastal Ocean Dynamics Experiment (CODE) region. WHOI, Tech. Rep. 83-25, 44 pp.

Champagne, F. H., C. A. Friehe, J. C. LaRue and J. C. Wyngaard, 1977: Flux measurement, flux estimation techniques, and fine-scale turbulence measurements in the unstable surface layer over land. *J. Atmos. Sci.,* **34,** 515–530.

Csanady, G. T., 1978: The arrested topographic wave. *J. Phys. Oceanogr.*, **8**, 47–62.

Deacon, E. L., 1959: The measurement of turbulent transfer in the lower atmosphere. *Advances in Geophysics,* Vol. 6, Academic Press, 211–228.

Donelan, M. A., S. A. Kitaigorodskii, J. L. Lumley and E. A. Terray, 1983: Wave turbulence interactions in the upper Ocean. Part II: Statistical characteristics of wave and turbulent components of random velocity field in the marine surface layer. *J. of Phys. Oceanogr.*, **13**, 1988–1999.

Forristall, G. Z., R. C. Hamilton and V. T. Cardone, 1977: Continental shelf currents in tropical storm Delia: Observations and theory. *J. Phys. Oceanogr.*, **7**, 532–536.

Glenn, S. M., 1983: "A continental shelf bottom boundary layer model: The effects of waves, currents and moveable bed." Sc.D thesis, WHOI-MIT Joint Program in Oceanography and Ocean Engineering, WHOI-83-6, 237 pp.

Grant, H. L., R. W. Stewart and A. Moilliet, 1962: Turbulence spectra from a tidal channel. *J. Fluid Mech.*, **12**, 238–266.

Grant, W. D., 1977: Bottom friction under waves in the presence of a weak current: Its relationship to coastal sediment transport. Sc.D. thesis, Massachusetts Institute of Technology, 275 pp.

——, 1982: The influence of internal waves on near bottom velocity profiles measured on the continental shelf: Stress and roughness estimates." *EOS Trans. Amer. Geophys. Union,* Vol. 63, No. 45, 987.

——, and O. S. Madsen, 1979: Combined wave and current interaction with a rough bottom. *J. Geophys. Res.*, **84**, 1797–1808.

——, and ——, 1982: Moveable bed roughness in unsteady oscillatory flow. *J. Geophys. Res.*, **87**, 469–481.

——, and S. M. Glenn, 1983: A Continental Shelf Bottom Boundary Layer Model; Volume I: Theoretical Development. Tech. Rep. to the American Gas Association, Woods Hole Oceanographic Institution, 167 pp.

——, A. J. Williams, III, S. M. Glenn, D. A. Cacchione and D. A. Drake, 1983: High Frequency Bottom Stress Variability and its Prediction at the CODE Site. Woods Hole Oceanographic Institution Tech. Rep. No. 83-19, 71 pp.

——, J. N. Newman and A. J. Williams: Calibration of an acoustic travel time current meter for ocean bottom boundary layer studies. (in preparation).

Gross, T. F., and A. R. M. Nowell, 1983: Mean Flow and Turbulence Scaling in a Tidal Boundary Layer. *Continental Shelf Research,* Vol. 2, 109–126.

Hinze, J. O., 1975: *Turbulence,* McGraw-Hill, 586 pp.

Jackson, P. S., 1981: On the displacement height in the logarithmic velocity profile. *J. Fluid Mech.*, **111**, 15–25.

Kemp, P. H., and R. R. Simons, 1982: "The interaction between waves and a turbulent current: Waves propagating with the current." *J. Fluid Mech.*, **116**, 227–250.

Long, C. E., 1981: A simple model for time-dependent stably stratified turbulent boundary layer. Special Rep. No. 95, Dept. of Oceanography, University of Washington, 170 pp.

Lumley, J. L., 1965: Interpretation of time spectra measured in high intensity shear flows. *Phys. of Fluids,* **8**, 1056–1062.

——, and E. A. Terray, 1983: Frequency spectra of frozen turbulence in a random wave field. *J. Phys. Oceanogr.*, **13**, 2000–2007.

Nagata, Y., 1964: The statistical properties of orbital wave motions and their application for the measurements of directional wave spectra. *J. Oceanogr. Soc. Japan,* **19**, 169–182.

Poala, C., 1983: Flow and Skin Friction over Naturally Rough Beds. PhD. thesis, WHOI-MIT Joint Program in Oceanography and Ocean Engineering. WHOI No. 83-18, 347 pp.

Smith, J. D., 1977: Modeling of sediment transport on continental shelves. *The Sea,* Vol. 6. Wiley-Interscience, 539–577.

——, and C. E. Long, 1976: The effect of turning in the bottom boundary layer on continental shelf sediment transport. *Mem. Soc. R. Sci. Liege,* Ser. 6, **10**, 369–396.

Tennekes, H., 1973: The logarithmic wind profile. *J. Atmos. Sci.*, **30**, 234–238.

Townsend, A. A., 1970: Entrainment and the structure of turbulent flow. *J. Fluid Mech.*, **41**, 13–46.

Trowbridge, J., 1983: Wave induced flow near a rough bed: Implications of a time-varying eddy viscosity. PhD. thesis, WHOI-MIT Joint Program in Oceanography and Ocean Engineering, 247 pp.

Wiberg, P., and J. D. Smith, 1983: A comparison of field data and theoretical models for wave-current interactions at the bed on the continental shelf. *Continental Shelf Research,* Vol. 2, 126–136.

Williams, A. J., and R. Kochler: An acoustic travel time current meter for ocean boundary layer measurements. (in preparation).

Winant, C. D., and R. C. Beardsley, 1979: A comparison of some shallow wind-driven currents. *J. Phys. Oceanogr.*, **9**, 218–220.

Wooding, R. A., E. F. Bradley and J. K. Marshall, 1973: Drag due to regular arrays of roughness elements of varying geometry. *Bound.-Layer Meteor.*, **5**, 285–308.